

# Power Control in Cellular Massive MIMO with Varying User Activity: A Deep Learning Solution

Trinh Van Chien, *Student Member, IEEE*, Thuong Nguyen Canh, *Student Member, IEEE*,  
Emil Björnson, *Senior Member, IEEE*, and Erik G. Larsson, *Fellow, IEEE*

## Abstract

This paper demonstrates how neural networks can be used to perform efficient joint pilot and data power control in multi-cell Massive MIMO systems, by exploiting the problem structure. We first consider the sum spectral efficiency (SE) optimization problem for systems with a dynamically varying number of active users. Since this problem is non-convex, an iterative algorithm is first derived to obtain a stationary point in polynomial time. We then use this algorithm together with deep learning to achieve an implementation that provable can be used in real-time applications. The proposed neural network, PowerNet, only uses the large-scale fading information to predict both pilot and data powers. One key feature is that PowerNet can manage a dynamically changing number of users per cell without requiring retraining, which is not the case in prior works and thus makes PowerNet an important step towards a practically useful solution. Numerical results demonstrate that PowerNet only loses 2% in sum SE, compared to the iterative algorithm, in a nine-cell system with up to 90 active users per in each coherence interval, and the runtime was only 0.03 ms on a graphics processing unit (GPU).

## Index Terms

Massive MIMO, Pilot and Data Power Control, Deep Learning, Convolutional Neural Network.

## I. INTRODUCTION

Future networks must provide higher channel capacity, lower latency, and better quality of service than contemporary networks [2]. These goals can only be achieved by drastic improvements

T. V. Chien, E. Björnson, and E. G. Larsson are with the Department of Electrical Engineering (ISY), Linköping University, 581 83 Linköping, Sweden (email: trinh.van.chien@liu.se; emil.bjornson@liu.se; erik.g.larsson@liu.se). T. N. Canh is with the Department of Electrical and Computer Engineering, Sungkyunkwan University, Suwon 440-746, Korea (e-mail: ngcthuong@skku.edu). Parts of this paper will be presented at ICC 2019 [1].

This paper was supported by the European Union's Horizon 2020 research and innovation programme under grant agreement No 641985 (5Gwireless). It was also supported by ELLIIT and CENIIT.

of the wireless network architecture [3]. Among potential candidates, Massive MIMO (multiple-input multiple-output) is an emerging physical layer technology which allows a base station (BS) equipped with many antennas to serve tens of users on the same time and frequency resource [4]. Utilizing the same spectrum and power budget, Massive MIMO can increase both spectral and energy efficiency by orders of magnitude compared with the conventional systems that are used today. This is because the propagation channels decorrelate when increasing the number of antennas at each BS and strong array gains are achievable with little inter-user interference.

Resource allocation is important in Massive MIMO networks to deal with the inter-user interference and, particularly, so-called pilot contamination [5]. Many resource allocation problems in Massive MIMO are easier to solve than in conventional systems since the channel hardening makes the utility functions only depend on the large-scale fading coefficients which are stable over a long time period [6], while adaptation to the quickly varying small-scale fading is conventionally needed. Table I categorizes the existing works on power control for cellular Massive MIMO in terms of utility functions and optimization variables. There are only a few works that jointly optimize the pilot and data powers, which is of key importance to deal with pilot contamination in multi-cell systems. In this paper, we optimize the sum SE with respect to the pilot and data powers. To the best of our knowledge, it is the first paper that considers this problem in cellular Massive MIMO systems, where each BS serves a varying number of users. Note that we did not include single-cell papers in Table I. For example, the paper [7] exploits the special structure arising from imperfect channel state information (CSI) in single-cell systems to maximize the sum SE using an efficient algorithm. This algorithm finds the globally optimal pilot and data powers, but it does not extend to multi-cell systems since the structure is entirely different.

Deep learning [8] is a popular data-driven approach to solve complicated problems and has shown superior performance in various applications in image restoration, pattern recognition, etc. Despite its complicated and rather heuristic training phase, deep learning has recently shown promising results in communication applications [9]. From the universal approximation theorem [10], deep learning can learn to approximate functions for which we have no closed-form expression. The authors in [11] construct a fully-connected deep neural network for the sum SE maximization problem for a wireless system serving a few tens of users. This network structure is reused in [12] to solve an energy-efficiency problem. Standard fully connected feed-forward networks with many layers are used, but since the considered problems are challenging, the prediction performance is much lower than when directly solving the optimization problems,

TABLE I  
PREVIOUS WORKS ON POWER CONTROL FOR CELLULAR MASSIVE MIMO

Variables Utility function	Data Powers Only	Joint Pilot & Data
Minimum transmit power	[13]–[15]	[16]
Max-min fairness	[14], [15], [17]–[19]	[20], [21]
Maximum product SINR	[14], [19]	[22]
Maximum sum SE	[23]–[25]	<b>This paper</b>

e.g., the loss varies from 5% to 16% depending on the system setting.

Moreover, previous neural network designs for resource allocation in wireless communications are utilizing the instantaneous channel state information (CSI) which is practically questionable, especially in cellular Massive MIMO systems. This is because the small-scale fading varies very quickly and the deep neural networks have very limited time to process the collection of all the instantaneous channel vectors, each having a number of parameters proportional to the number of BS antennas. The recent work in [19] designs a neural network utilizing only statistical channel information to predict transmit powers in an equally-loaded cellular Massive MIMO system with spatially correlated fading. Although the prediction performance is good, the paper does not discuss how to generalize the approach to having varying number of users per cell. If there are  $L$  cells and between 0 and  $K_{\max}$  users per cell, the naive approach would be to train  $L2^{K_{\max}}$  different neural networks to cover all cases that can appear. Even in the small setup of  $L = 4$  and  $K_{\max} = 5$  considered in [19], this requires 128 different neural networks. Therefore this is not practical for large-scale cellular systems. A better generalization would be to train the networks to manage a varying number of interfering users in other cells, but this still requires  $K_{\max}$  neural networks per cell and the performance loss is hard to predict. In contrast, the proposed approach in this paper only require one neural network.

In this paper, we consider the joint optimization of the pilot and data powers for maximum sum SE in multi-cell Massive MIMO systems. Our main contributions are:

- We formulate a sum ergodic SE maximization problem, with the data and pilot powers as variables, where each cell may have a different number of active users. To overcome the inherent non-convexity, an equivalent problem with element-wise convex structure is derived. An alternating optimization algorithm is proposed to find a stationary point. Each iteration is solved in closed form.
- We design a deep convolutional neural network (CNN) that learns the solution to the alter-

nating optimization algorithm. The inputs to the CNN are the large-scale fading coefficients between each user and BS, while the outputs are the pilot and data powers. Hence, the number of inputs/outputs is independent of the number of antennas. Our deep CNN is named PowerNet, has a residual structure, and is densely connected.

- We exploit the structure of the sum SE maximization problem to train PowerNet to handle a varying number of users per cell. Hence, in contrast to prior works, a single PowerNet is sufficient irrespective of the number of active users, and no retraining is needed.
- Numerical results manifest the effectiveness of the proposed alternating optimization algorithm as compared to the baseline of full transmit power. Meanwhile, PowerNet achieves highly accurate power prediction and a sub-milliseconds runtime.

The remainder of this paper is organized as follows: Section II introduces our cellular Massive MIMO system model, with a varying number of users per cell, and the basic ergodic SE analysis. We formulate and solve the joint pilot and data power control problem for maximum sum SE in Section III. The proposed low complexity deep learning solution is given in Section IV. Finally, numerical results are shown in Section V and we provide the main conclusions in Section VI.

*Notation:* Upper (lower) bold letters are used to denote matrices (vectors).  $\mathbb{E}\{\cdot\}$  is the expectation of a random variable.  $(\cdot)^H$  is the Hermitian transpose and the cardinality of set  $\mathcal{A}$  is  $|\mathcal{A}|$ . We let  $\mathbf{I}_M$  denote the  $M \times M$  identity matrix.  $\mathbb{C}, \mathbb{R}$ , and  $\mathbb{R}_+$  denote the complex, real and non-negative real field, respectively. The floor operator denotes as  $\lfloor \cdot \rfloor$  and the Frobenius norm as  $\|\cdot\|_F$ . Finally,  $\mathcal{CN}(\cdot, \cdot)$  is circularly symmetric complex Gaussian distribution.

## II. DYNAMIC MASSIVE MIMO SYSTEM MODEL

We consider a multi-cell Massive MIMO system comprising of  $L$  cells, each having a BS equipped with  $M$  antennas. We call it a dynamic system model since each BS is able to serve  $K_{\max}$  users, but maybe only a subset of the users are active at any given point in time. We will later model the active subset of users randomly and exploit this structure when training a neural network. Since the wireless channels vary over time and frequency, we consider the standard block fading model [17] where the time-frequency resources are divided into coherence intervals of  $\tau_c$  modulation symbols for which the channels are static and frequency flat. At an arbitrary given coherence interval, BS  $l$  is serving a subset of active users. We define a set  $\mathcal{A}_l$  containing the indices of all active users in cell  $l$ , for which  $0 \leq |\mathcal{A}_l| \leq K_{\max}$ . The channel between active user  $t \in \mathcal{A}_l$  in cell  $i$  and BS  $l$  is denoted as  $\mathbf{h}_{i,t}^l \in \mathbb{C}^M$  and follows an independent and identically distributed (i.i.d.) Rayleigh fading distribution:

$$\mathbf{h}_{i,t}^l \sim \mathcal{CN}(\mathbf{0}, \beta_{i,t}^l \mathbf{I}_M), \quad (1)$$

where  $\beta_{i,t}^l \geq 0$  is the large-scale fading coefficient that models geometric pathloss and shadow fading. The distributions are known at the BSs, but the realizations are unknown and need to be estimated in every coherence interval using a pilot transmission phase.

#### A. Uplink Pilot Transmission Phase

We assume that a set of  $K_{\max}$  orthonormal pilot signals are used in the system. User  $k$  in each cell is preassigned the pilot  $\boldsymbol{\psi}_k \in \mathbb{C}^{K_{\max}}$  with  $\|\boldsymbol{\psi}_k\|^2 = K_{\max}$ , no matter if the user is active or not in the given coherence interval, but this pilot is only transmitted when the user has data to transmit (or receive). This pilot assignment guarantees that there is no intra-cell pilot contamination. The channel estimation of a user is interfered by the users that use the pilot signal, which is called pilot contamination. The received baseband pilot signal  $\mathbf{Y}_l \in \mathbb{C}^{M \times K_{\max}}$  at BS  $l$  is

$$\mathbf{Y}_l = \sum_{i=1}^L \sum_{t \in \mathcal{A}_i} \sqrt{\hat{p}_{i,t}} \mathbf{h}_{i,t}^l \boldsymbol{\psi}_t^H + \mathbf{N}_l, \quad (2)$$

where  $\mathbf{N}_l \in \mathbb{C}^{M \times K}$  is the additive noise with i.i.d.  $\mathcal{CN}(0, \sigma_{\text{UL}}^2)$  elements. Meanwhile,  $\hat{p}_{i,t}$  is the pilot power that active user  $t$  in cell  $i$  allocates to its pilot transmission. The channel between a particular user  $t \in \mathcal{A}_i$  in cell  $i$  and BS  $l$  is estimated from

$$\mathbf{y}_{i,t} = \mathbf{Y}_l \boldsymbol{\psi}_t = \sum_{i' \in \mathcal{P}_t} \sqrt{\hat{p}_{i',t}} \mathbf{h}_{i',t}^l \boldsymbol{\psi}_t^H \boldsymbol{\psi}_t + \mathbf{N}_l \boldsymbol{\psi}_t, \quad (3)$$

where the set  $\mathcal{P}_t$  contains the indices of cells having user  $t$  in active mode, which is formulated from the user activity set of each cell as

$$\mathcal{P}_t = \{i' \in \{1, \dots, L\} : t \in \mathcal{A}_{i'}\}. \quad (4)$$

By using minimum mean square error (MMSE) estimation [26], the channel estimate of an arbitrary active user is as follows.

**Lemma 1.** *If BS  $l$  uses MMSE estimation, the channel estimate of active user  $t$  in cell  $i$  is*

$$\hat{\mathbf{h}}_{i,t}^l = \mathbb{E} \{ \mathbf{h}_{i,t}^l | \mathbf{y}_{i,t} \} = \frac{\beta_{i,t}^l \sqrt{\hat{p}_{i,t}}}{K_{\max} \sum_{i' \in \mathcal{P}_t} \hat{p}_{i',t} \beta_{i',t}^l + \sigma_{\text{UL}}^2} \mathbf{y}_{i,t}, \quad (5)$$

which follows a complex Gaussian distribution as

$$\hat{\mathbf{h}}_{i,t}^l \sim \mathcal{CN} \left( \mathbf{0}, \frac{K_{\max} (\beta_{i,t}^l)^2 \hat{p}_{i,t}}{K_{\max} \sum_{i' \in \mathcal{P}_t} \hat{p}_{i',t} \beta_{i',t}^l + \sigma_{\text{UL}}^2} \mathbf{I}_M \right). \quad (6)$$

By denoting the estimation error as  $\mathbf{e}_{i,t}^l = \mathbf{h}_{i,t}^l - \hat{\mathbf{h}}_{i,t}^l$ , then it is independently distributed as

$$\mathbf{e}_{i,t}^l \sim \mathcal{CN} \left( \mathbf{0}, \frac{K_{\max} \sum_{i' \in \mathcal{P}_t \setminus \{i\}} \hat{p}_{i',t} \beta_{i',t}^l \beta_{i,t}^l + \beta_{i,t}^l \sigma_{\text{UL}}^2}{K_{\max} \sum_{i' \in \mathcal{P}_t} \hat{p}_{i',t} \beta_{i',t}^l + \sigma_{\text{UL}}^2} \mathbf{I}_M \right). \quad (7)$$

*Proof.* The proof follows directly from standard MMSE estimation techniques [14], [26].  $\square$

The statistical information in Lemma 1 of each channel estimate and estimation error are used to construct the linear combining vectors and to derive a closed-form expression of the uplink SE.

### B. Uplink Data Transmission Phase

During the uplink data transmission phase, every active user  $t \in \mathcal{A}_i$  in cell  $i$  transmits data symbol  $s_{i,t}$  with  $\mathbb{E}\{|s_{i,t}|^2\} = 1$ . The received signal  $\mathbf{y}_l \in \mathbb{C}^M$  at BS  $l$  is the superposition of signals from all users across cells:

$$\mathbf{y}_l = \sum_{i=1}^L \sum_{t \in \mathcal{A}_i} \sqrt{p_{i,t}} \mathbf{h}_{i,t}^l s_{i,t} + \mathbf{n}_l, \quad (8)$$

where  $p_{i,t}$  is the power that active user  $t$  in cell  $i$  allocates to the data symbol  $s_{i,t}$  and  $\mathbf{n}_l \in \mathbb{C}^M$  is complex Gaussian noise distributed as  $\mathcal{CN}(\mathbf{0}, \sigma_{\text{UL}}^2 \mathbf{I}_M)$ . Each BS uses maximum ratio combining (MRC) to detect the desired signals from its users. In particular, BS  $l$  selects the combining vector for its user  $k$  as

$$\mathbf{v}_{l,k} = \hat{\mathbf{h}}_{l,k}^l, \quad (9)$$

and we will quantify the achievable spectral efficiency by using the use-and-then-forget capacity bounding technique [17]. The closed-form expression of the lower bound on the uplink capacity is shown in Lemma 2.

**Lemma 2.** *If each BS uses MRC for data detection, a closed-form expression for the uplink ergodic SE of active user  $k$  in cell  $l$  is*

$$R_{l,k}(\{\hat{p}_{i,t}, p_{i,t}\}) = \left(1 - \frac{K_{\max}}{\tau_c}\right) \log_2(1 + \text{SINR}_{l,k}), \quad (10)$$

where the effective SINR value of this user is

$$\text{SINR}_{l,k} = MK_{\max} p_{l,k} \hat{p}_{l,k} (\beta_{l,k}^l)^2 / D_{l,k} \quad (11)$$

and

$$D_{l,k} = MK_{\max} \sum_{i \in \mathcal{P}_k \setminus \{l\}} p_{i,k} \hat{p}_{i,k} (\beta_{i,k}^l)^2 + \left( K_{\max} \sum_{i \in \mathcal{P}_k} \hat{p}_{i,k} \beta_{i,k}^l + \sigma_{\text{UL}}^2 \right) \left( \sum_{i=1}^L \sum_{t \in \mathcal{A}_i} p_{i,t} \beta_{i,t}^l + \sigma_{\text{UL}}^2 \right). \quad (12)$$

*Proof.* The proof follows along the lines of Corollary 4.5 in [14] except for the different notation and the fact that every user can assign different power to pilot and data.  $\square$

The numerator of the SINR expression in (11) indicates contributions of the array gain which is directly proportional to the number of antennas at the serving BS. The first part in the denominator represents the pilot contamination effect and it is also proportional to the number of BS antennas. Interestingly, active user  $k$  in cell  $l$  will have unbounded capacity when  $M \rightarrow \infty$  if all users using the same pilot sequence  $\psi_k$  are silent (i.e., inactive or allocated zero transmit power), thanks to the massive antenna array gain while inter-cell mutual interference and noise are negligible. We notice that the remaining terms are non-coherent mutual interference and noise that can have a vanishing impact when the number of antennas grow. Furthermore, the SE of a user is proportional to  $(1 - K_{\max}/\tau_c)$ , which is the pre-log factor in (10). This is the fraction of symbols per coherence interval that are used for data transmission, which thus reduces when the number of pilots is increased. In the special case of  $|\mathcal{A}_1| = \dots = |\mathcal{A}_L|$ , the analytical results in Lemma 2 particularize to equally-loaded systems as in the previous works. That special case is unlikely to occur in practice since the data traffic is generated independently for each user.

### III. JOINT PILOT AND DATA POWER CONTROL FOR SUM SPECTRAL EFFICIENCY OPTIMIZATION

We are concerned with sum SE maximization since high SE is important for future networks, and the (weighted) sum SE maximization is also the core problem to be solved in practical algorithms for dynamic resource allocation [27]. The previous works [7], [25] consider this problem for single-cell systems with joint pilot and data power control or multi-cell systems with only data power control, respectively. In contrast, we formulate and solve a sum SE maximization problem with joint pilot and data power control. This optimization problem has not been tackled before in the Massive MIMO literature due to its inherent non-convexity structure. In this section, we develop an iterative algorithm that achieves a stationary point in polynomial time by solving a series of convex sub-problems in closed form.

#### A. Problem Formulation

We consider the optimization problem that maximizes the sum SE of all active users in the system with limited power at each transmitted symbol as

$$\begin{aligned}
 & \underset{\{\hat{p}_{l,k}, p_{l,k} \geq 0\}}{\text{maximize}} && \sum_{l=1}^L \sum_{k \in \mathcal{A}_l} R_{l,k}(\{\hat{p}_{i,t}, p_{i,t}\}) \\
 & \text{subject to} && \hat{p}_{l,k} \leq P_{l,k}, \quad \forall l, k, \\
 & && p_{l,k} \leq P_{l,k}, \quad \forall l, k,
 \end{aligned} \tag{13}$$

where  $P_{l,k} \geq 0$  is the maximum power that user  $k$  in cell  $l$  can supply to each transmitted symbol. Problem (13) is independent of the small-scale fading, so it allows for long-term performance optimization, if the users are continuously active and there is no large-scale user mobility. However, in practical systems, some users are moving quickly and new scheduling decisions are made every few milliseconds based on the users' traffic. It is therefore important to be able to solve (13) very quickly to adapt to these changes.<sup>1</sup> The sum SE optimization problem is non-convex in general and seeking the optimal solution has very high complexity in any non-trivial setup [28]. However, the pilot and data power constraints in (13) guarantee a convex feasible set and make all ergodic SE expressions continuous functions of the power variables. According to Weierstrass theorem [29], an optimal solution set of pilot and data power coefficients always exists.

Inspired by the weighted MMSE methodology [30], we will now propose an iterative algorithm to find a stationary point to (13). By removing the pre-log factor and setting  $\hat{\rho}_{l,k} = \sqrt{\hat{p}_{l,k}}$  and  $\rho_{l,k} = \sqrt{p_{l,k}}, \forall l, k$ , as the new optimization variables, we formulate a new problem that is equivalent with (13).

**Theorem 1.** *The following optimization problem is equivalent to problem (13):*

$$\begin{aligned} & \underset{\substack{\{w_{l,k} \geq 0, u_{l,k}\}, \\ \{\hat{\rho}_{l,k}, \rho_{l,k} \geq 0\}}}{\text{minimize}} && \sum_{l=1}^L \sum_{k \in \mathcal{A}_l} w_{l,k} e_{l,k} - \ln(w_{l,k}) \\ & \text{subject to} && \hat{\rho}_{l,k}^2 \leq P_{l,k}, \quad \forall l, k, \\ & && \rho_{l,k}^2 \leq P_{l,k}, \quad \forall l, k, \end{aligned} \quad (14)$$

where

$$\begin{aligned} e_{l,k} = & MK_{\max} u_{l,k}^2 \sum_{i \in \mathcal{P}_k} \rho_{i,k}^2 \hat{\rho}_{i,k}^2 (\beta_{i,k}^l)^2 - 2\sqrt{MK_{\max}} \rho_{l,k} \hat{\rho}_{l,k} u_{l,k} \beta_{l,k}^l \\ & + u_{l,k}^2 \left( K_{\max} \sum_{i \in \mathcal{P}_k} \hat{\rho}_{i,k}^2 \beta_{i,k}^l + \sigma_{\text{UL}}^2 \right) \left( \sum_{i=1}^L \sum_{t \in \mathcal{A}_i} \rho_{i,t}^2 \beta_{i,t}^l + \sigma_{\text{UL}}^2 \right) + 1, \end{aligned} \quad (15)$$

in the sense that if  $\{u_{l,k}^*, w_{l,k}^*, \hat{\rho}_{l,k}^*, \rho_{l,k}^*\}$  is a global optimum to problem (14), then  $\{(\hat{\rho}_{l,k}^*)^2, (\rho_{l,k}^*)^2\}$  is a global optimum to problem (13).

*Proof.* The proof consists of two main steps: the mean square error  $e_{l,k}$  is first formulated by considering a single-input single-output (SISO) communication system with deterministic

<sup>1</sup>Note that the ergodic SE is a reasonable performance metric also in this scenario, since long codewords can span over the frequency domain and the channel hardening makes the channel after MRC almost deterministic. The simulations in [6] shows that coding over 1 kB of data is sufficient to operate closely to the ergodic SE.



---

**Algorithm 1** Alternating optimization approach for (14)

---

**Input:** Large-scale fading  $\beta_{i,t}^l, \forall i, t, l$ ; Maximum power levels  $P_{l,k}, \forall l, k$ ; Initial values  $\hat{\rho}_{l,k}^{(0)}$  and  $\rho_{l,k}^{(0)}, \forall l, k$ . Set up  $n = 1$ .

1. *Iteration n:*

1.1. Update the variables  $u_{l,k}^{(n)}$ , for all  $l, k$ , by using (16) where every  $\tilde{u}_{l,k}^{(n-1)}$  is computed as in (17).

1.2. Update the variables  $w_{l,k}^{(n)}$ , for all  $l, k$ , by using (18) where every  $e_{l,k}^{(n)}$  is computed as in (19).

1.3. Update the variables  $\hat{\rho}_{l,k}^{(n)}$ , for all  $l, k$ , by using (20).

1.4. Update the variables  $\rho_{l,k}^{(n)}$ , for all  $l, k$ , by using (22).

2. If *Stopping criterion* (24) is satisfied  $\rightarrow$  Stop. Otherwise, go to Step 3.

3. Store the currently solution:  $\hat{\rho}_{l,k}^{(n)}$  and  $\rho_{l,k}^{(n)}, \forall l, k$ . Set  $n = n + 1$ , then go to Step 1.

**Output:** The stationary point:  $\hat{\rho}_{l,k}^{\text{opt}} = \rho_{l,k}^{(n)}, \rho_{l,k}^{\text{opt}} = \rho_{l,k}^{(n)} \forall l, k$ .

---

channels having the same SE as in Lemma 2, where  $u_{l,k}$  is the beamforming coefficient utilized in such a SISO system and  $w_{l,k}$  is the weight value in the receiver. After that, the equivalence of two problems (13) and (14) is obtained by finding the optimal solution of  $u_{l,k}$  and  $w_{l,k}, \forall l, k$ , given the other optimization variables. The detailed proof is given in Appendix A.  $\square$

The new problem formulation in Theorem 1 is still non-convex, but it has an important desired property: if we consider one of the sets  $\{u_{l,k}\}, \{w_{l,k}\}, \{\hat{\rho}_{l,k}\}$ , and  $\{\rho_{l,k}\}$  as the only optimization variables, while the other variables are constant, then problem (15) is convex. Note that the set of optimization variables and SE expressions are different than in the previous works [31], [32] that followed similar paths of reformulating their sum SE problems, which is why Theorem 1 is a main contribution of this paper. In particular, in our case we can get closed-form solutions in each iteration, leading to a particularly efficient implementation. We exploit this property to derive an iterative algorithm to find a local optimum (stationary point) to (15) as shown in the following subsection.

### B. Iterative Algorithm

This subsection provides an iterative algorithm to obtain a stationary point to problem (14) by alternating between updating the different sets of optimization variables. This procedure is established by the following theorem.

**Theorem 2.** From an initial point  $\{\hat{\rho}_{l,k}^{(0)}, \rho_{l,k}^{(0)}\}$  satisfying the constraints, a stationary point to problem (14) is obtained by updating  $\{u_{l,k}, w_{l,k}, \hat{\rho}_{l,k}, \rho_{l,k}\}$  in an iterative manner. At iteration  $n$ , the variables are updated as follows:

- The  $u_{l,k}$  variables, for all  $l, k$ , are updated as

$$u_{l,k}^{(n)} = \sqrt{MK_{\max}} \rho_{l,k}^{(n-1)} \hat{\rho}_{l,k}^{(n-1)} \beta_{l,k}^l / \tilde{u}_{l,k}^{(n-1)}, \quad (16)$$

where

$$\tilde{u}_{l,k}^{(n-1)} = MK_{\max} \sum_{i \in \mathcal{P}_k} (\rho_{i,k}^{(n-1)})^2 (\hat{\rho}_{i,k}^{(n-1)})^2 (\beta_{i,k}^l)^2 + \left( K_{\max} \sum_{i \in \mathcal{P}_k} (\hat{\rho}_{i,k}^{(n-1)})^2 \beta_{i,k}^l + \sigma_{\text{UL}}^2 \right) \times \left( \sum_{i=1}^L \sum_{t \in \mathcal{A}_i} (\rho_{i,t}^{(n-1)})^2 \beta_{i,t}^l + \sigma_{\text{UL}}^2 \right). \quad (17)$$

- The variables  $w_{l,k}$ , for all  $l, k$ , are updated as

$$w_{l,k}^{(n)} = 1/e_{l,k}^{(n)}, \quad (18)$$

where

$$e_{l,k}^{(n)} = (u_{l,k}^{(n)})^2 \tilde{u}_{l,k}^{(n-1)} - 2\sqrt{MK_{\max}} \rho_{l,k}^{(n-1)} \hat{\rho}_{l,k}^{(n-1)} u_{l,k}^{(n)} \beta_{l,k}^l + 1. \quad (19)$$

- The variables  $\hat{\rho}_{l,k}$ , for all  $l, k$ , are updated as in (20).

$$\hat{\rho}_{l,k}^{(n)} = \min \left( \frac{\sqrt{MK_{\max}} \rho_{l,k}^{(n-1)} u_{l,k}^{(n)} w_{l,k}^{(n)} \beta_{l,k}^l}{\hat{\eta}_{l,k}^{(n)}}, \sqrt{P_{l,k}} \right), \quad (20)$$

where  $\hat{\eta}_{l,k}^{(n)}$  is given by

$$\hat{\eta}_{l,k}^{(n)} = (\rho_{l,k}^{(n-1)})^2 MK_{\max} \sum_{i \in \mathcal{P}_k} w_{i,k}^{(n)} (u_{i,k}^{(n)})^2 (\beta_{i,k}^l)^2 + K_{\max} \sum_{j \in \mathcal{P}_k} w_{j,k}^{(n)} (u_{j,k}^{(n)})^2 \beta_{l,k}^j \times \left( \sum_{i=1}^L \sum_{t \in \mathcal{A}_i} (\rho_{i,t}^{(n)})^2 \beta_{i,t}^j + \sigma_{\text{UL}}^2 \right). \quad (21)$$

- The variables  $\rho_{l,k}$ , for all  $l, k$ , are updated as in (22).

$$\rho_{l,k}^{(n)} = \min \left( \frac{\sqrt{MK_{\max}} \hat{\rho}_{l,k}^{(n)} u_{l,k}^{(n)} w_{l,k}^{(n)} \beta_{l,k}^l}{\eta_{l,k}^{(n)}}, \sqrt{P_{l,k}} \right), \quad (22)$$

where  $\eta_{l,k}^{(n)}$  is given by

$$\eta_{l,k}^{(n)} = (\hat{\rho}_{l,k}^{(n)})^2 MK_{\max} \sum_{i \in \mathcal{P}_k} w_{i,k}^{(n)} (u_{i,k}^{(n)})^2 (\beta_{i,k}^l)^2 + \sum_{i=1}^L \sum_{t \in \mathcal{A}_i} w_{i,t}^{(n)} (u_{i,t}^{(n)})^2 \beta_{l,k}^i \times \left( K_{\max} \sum_{j \in \mathcal{P}_k} (\hat{\rho}_{j,t}^{(n)})^2 \beta_{j,t}^i + \sigma_{\text{UL}}^2 \right). \quad (23)$$

This iterative process converges to a stationary point  $\{u_{l,k}^{\text{opt}}, w_{l,k}^{\text{opt}}, \hat{\rho}_{l,k}^{\text{opt}}, \rho_{l,k}^{\text{opt}}\}$  to problem (14) and then  $\{(\hat{\rho}_{l,k}^{\text{opt}})^2, (\rho_{l,k}^{\text{opt}})^2\}$  is also a stationary point to problem (13).

*Proof.* The proof derives the closed-form optimal solutions in (16)–(22) to each of the optimization variables, when the other are fixed, by taking the first derivative of the Lagrangian function of (14) and equating it to zero. The fact that problems (13) and (14) have the same set of stationary points is further confirmed by the chain rule. The proof is given in Appendix B.  $\square$

Theorem 2 provides an iterative algorithm that obtains a local optimum to (13) and (14) with low computational complexity because of the closed-form solutions in each iteration. Algorithm 1 gives a summary of this iterative process. From any feasible initial set of powers  $\{\hat{\rho}_{l,k}^{(0)}, \rho_{l,k}^{(0)}\}$ , in each iteration, we update each optimization variable according to (16)–(22). This iterative process will be terminated when the variation of two consecutive iterations is small. For instance the stopping condition may be defined for a given accuracy  $\epsilon > 0$  as

$$\left| \sum_{l=1}^L \sum_{k \in \mathcal{A}_l} R_{l,k}^{(n)} - \sum_{l=1}^L \sum_{k \in \mathcal{A}_l} R_{l,k}^{(n-1)} \right| \leq \epsilon. \quad (24)$$

By considering the multiplications, divisions, and logarithms as the dominated complexity, the number of arithmetic operations need for Algorithm 1 to reach  $\epsilon$ -accuracy is

$$N_1 \left( 8 \sum_{i=1}^L |\mathcal{A}_i| + 4 |\mathcal{P}_k| \sum_{i=1}^L |\mathcal{A}_i| + 23 |\mathcal{P}_k| + 50 \right) \sum_{i=1}^L |\mathcal{A}_i|, \quad (25)$$

where  $N_1$  is the number iterations required for the convergence which depends on the given  $\epsilon$ -accuracy. From our experience with Rayleigh fading channels,  $N_1$  is on average about 100 to achieve the error bound less than  $\epsilon = 10^{-3}$ . From Theorem 2, we further observe the relationship of data and pilot power allocated to a user as the following.

**Corollary 1.** *If an active user has a large-scale fading coefficient equal to zero, then it will always get zero transmit powers when using the algorithm in Theorem 2. Hence, an equivalent way of managing inactive users is to set their large-scale fading coefficients to zero and use  $\mathcal{A}_i = \{1, \dots, K_{\max}\}$ .*

*Proof.* The numerators of (20) and (22) directly imply that any user with zero large-scale fading ( $\beta_{l,k}^l = 0$ ) will be allocated zero pilot power ( $\hat{p}_{l,k} = 0$ ) and zero data power ( $p_{l,k} = 0$ ).  $\square$

Note that, notwithstanding Corollary 1, the system may reject some active users that have small but non-zero large-scale fading coefficients since Algorithm 1 can assign zero power to these ones—similar to the behavior of standard waterfilling algorithms. This is a key benefit of

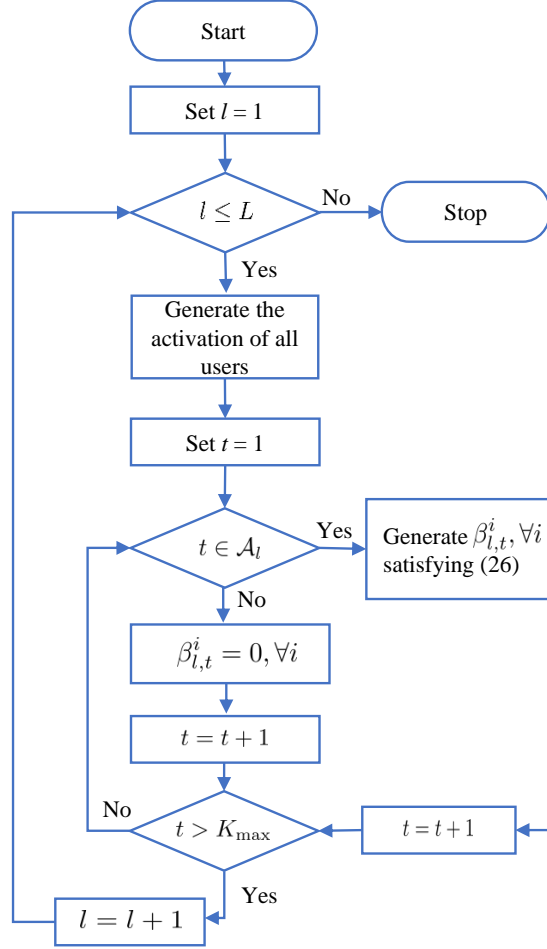


Fig. 1. The flowchart of generating one realization of the Massive MIMO network with  $LK_{\max}$  users having random large-scale fading realizations and activity.

sum SE maximization as compared to max-min fairness power control [14], [15], [17]–[21] and maximum product-SINR power control [14], [19], [22], which always allocate non-zero power to all users and, therefore, require an additional heuristic user admission control step for selecting which users to drop from service due to their poor channel conditions. If a particular user  $t$  in cell  $i$  is not served this implies that  $\hat{p}_{i,t}^{\text{opt}} = 0$  and  $p_{i,t}^{\text{opt}} = 0$ . Hence, this user is neither transmitting in the pilot nor data phase. Corollary 1 will enable us to design a single neural network that can mimic Algorithm 1 for any number of active users.

#### IV. A LOW-COMPLEXITY SOLUTION WITH CONVOLUTIONAL NEURAL NETWORK

In this section, we introduce a deep learning framework for joint pilot and data power allocation in dynamic cellular Massive MIMO systems, which uses supervised learning to mimic the power control obtained by Algorithm 1. We stress that for non-convex optimization problems, a supervised learning approach with high prediction accuracy is both useful for achieving a

low-complexity implementation, harnessing the advances in implementing neural networks on GPUs, and provides a good baseline for further activities, e.g., supervised learning as a warm start for unsupervised learning or to improve the performance of the testing phase [33].

We first make an explicit assumption on how the large-scale fading coefficients are generated for each realization of the Massive MIMO network, by exploiting Corollary 1.

**Assumption 1.** *We consider an  $L$ -cell system where the activation of each user is determined by an independent Bernoulli distribution with activity probability  $p \in [0, 1]$ . The large-scale fading coefficients associated with a user in cell  $l$  have the probability density function (PDF)  $f_l(\boldsymbol{\beta})$ , in which  $\boldsymbol{\beta} \in [0, 1]^L$  and  $[\boldsymbol{\beta}]_l = \max_{i \in \{1, \dots, L\}} [\boldsymbol{\beta}]_i$ , for  $l = 1, \dots, L$ .*

*In each realization of the system,  $K_{\max}$  i.i.d. users are generated in each cell. User  $t$  in cell  $l$  is active (i.e.,  $t \in \mathcal{A}_l$ ) with the probability  $p$ . Inactive users have  $\boldsymbol{\beta}_{l,k} = [\beta_{l,k}^1, \dots, \beta_{l,k}^L]^T = \mathbf{0}$  and the large-scale fading coefficients  $\boldsymbol{\beta}_{l,k} = [\beta_{l,k}^1, \dots, \beta_{l,k}^L]^T$  of active user is obtained as an i.i.d. realization with the PDF  $f_l(\cdot)$  that satisfies*

$$\beta_{l,t}^l = \max_{i \in \{1, \dots, L\}} \beta_{l,t}^i, \quad (26)$$

*such that it has its strongest channel from the serving BS.*

The process of generating system realizations is illustrated in Fig. 1. Note that all users in cell  $i$  have the same  $f_i(\cdot)$ , which represents the user distribution over the coverage area of this cell, but this function is different for each cell. For notational convenience, each cell has the same maximum number of users  $K_{\max}$  and the activity probability is independent of the cell and location, but these assumptions can be easily generalized.

Assumption 1 indicates that a user should be handled equally irrespective of which number that it has in the cell. The fact that all large-scale fading coefficients belong to compact set  $[0, 1]$  originates from the law of conservation of energy, and fits well with the structural conditions required to construct a neural networks [10]. There are many ways to define the PDFs of the large-scale fading coefficients. One option is to match them to channel measurements obtained in a practical setup [34]. Another option is to define the BS locations and user distributions and then define a pathloss model with shadow fading. In the numerical part of this paper, we take the latter approach and follow the 3GPP LTE standard [35] that utilizes a Rayleigh-lognormal fading model that matches well to channel measurements in non-line-of-sight conditions. The following model is used in Section V.

**Example 1.** Consider a setup with  $L$  square cells. In each cell, the  $K_{\max}$  users are uniformly distributed in the serving cell at distances to the serving BS that are larger than 35 m. Each user has the activity probability  $p = 2/3$ . For an active user  $t$  in cell  $l$ , we generate the large-scale fading coefficient to BS  $i$  as

$$\beta_{l,t}^i [\text{dB}] = -148.1 - 37.6 \log_{10}(d_{l,t}^i/1 \text{ km}) + z_{l,t}^i, \quad (27)$$

where  $d_{l,t}^i$  is the physical distance and  $z_{l,t}^i$  is shadow fading that follows a normal distribution with zero mean and standard derivation 7 dB. If the conditions (26) and/or  $\beta_{l,t}^i \leq 1$  are not satisfied for a particular user, we simply rerun all the shadow fading realizations for that user.

In a cellular network with  $LK_{\max}$  users there are  $L2^{K_{\max}}$  different possibilities of the deep neural networks, which is a big number (up to 9126 in the simulation part with 90 users). If we had to design all such specific neural networks, the solution is practically meaningless. A main contribution of our framework is that we can exploit the structure of the optimization problem to build a single neural network that can handle the activity/inactivity pattern and has a unified structure for all training samples. Note that the proposed network might have more parameters than actually needed, since our main goal is to provide a proof-of-concept. The network with the lowest number of parameters is different for every propagation environment and therefore not considered in this work, which focuses on the general properties and not the fine-tuning.

#### A. Existence of a Neural Network for Joint Pilot and Data Power Control

The input to the proposed feedforward neural network is only the large-scale fading coefficients and the output is the data and pilot powers. This is fundamentally different from previous works [11], [12] that use deep learning methods to predict the data power allocation based on perfect instantaneous CSI (i.e., small-scale fading), in which case no channel estimation is involved. Specifically, we define a tensor  $\mathbf{l} \in \mathbb{R}_+^{L \times L \times K_{\max}}$  containing all the large-scale fading coefficients. We let  $\mathbf{O}_d^{\text{opt}} \in \mathbb{R}_+^{L \times 1 \times K_{\max}}$  denote the tensor with optimized data powers and  $\mathbf{O}_p^{\text{opt}} \in \mathbb{R}_+^{L \times 1 \times K_{\max}}$  denote the tensor with pilot powers. PowerNet learns the continuous mapping<sup>2</sup>

$$\mathcal{F} \left( \mathbf{l}, \{\rho_{l,k}^{(0)}\}, \{\hat{\rho}_{l,k}^{(0)}\} \right) = \{\mathbf{O}_d^{\text{opt}}, \mathbf{O}_p^{\text{opt}}\}, \quad (28)$$

where  $\mathcal{F}(\cdot, \cdot, \cdot)$  represents the continuous mapping process in Algorithm 1 to obtain the stationary point from the input set of large-scale fading together with an initial set of pilot and data powers.

<sup>2</sup>The process  $h(\mathbf{x}) = [h_1(\mathbf{x}), \dots, h_{N_1}(\mathbf{x})]$  is a continuous mapping if all  $h_n(\mathbf{x}), \forall n \in \{1, \dots, N_1\}$ , are continuous functions.

Lemma 3 first proves the existence of a feedforward network which imitates the continuous mapping in (28).

**Lemma 3.** *For any given accuracy  $\delta > 0$ , there exists an integer  $S$  and a feedforward neural network  $\text{Net}_S(\mathbf{l}, \mathbf{f})$  with  $S$  hidden units for which the mapping process in (28) produces similar performance as Algorithm 1 in the sense that*

$$\sup_{\substack{\mathbf{f}, \{0 \leq p_{l,k} \leq P_{l,k}\}, \\ \{0 \leq \hat{p}_{l,k} \leq P_{l,k}\}}} \|\text{Net}_S(\mathbf{l}, \mathbf{f}) - \mathcal{F}(\mathbf{l}, \{\rho_{l,k}^{(0)}\}, \{\hat{\rho}_{l,k}^{(0)}\})\|_F \leq \delta, \quad (29)$$

where  $\mathbf{f}$  are the set of network parameters comprising kernels and biases. If we stack the data and pilot powers into the tensors  $\mathbf{O}_d, \mathbf{O}_p \in \mathbb{R}_+^{L \times 1 \times K_{\max}}$  such that  $[\mathbf{O}_d]_{l,1,k} = p_{l,k}$  and  $[\mathbf{O}_p]_{l,1,k} = \hat{p}_{l,k}, \forall l, k$ , then the objective function in the left-hand side of (29) can be rewritten as

$$\|\text{Net}_S(\mathbf{l}, \mathbf{f}) - \mathcal{F}(\mathbf{l}, \{\rho_{l,k}^{(0)}\}, \{\hat{\rho}_{l,k}^{(0)}\})\|_F = \|\mathbf{O}_d - \mathbf{O}_d^{\text{opt}}\|_F + \|\mathbf{O}_p - \mathbf{O}_p^{\text{opt}}\|_F. \quad (30)$$

*Proof.* The result is obtained by applying the universal approximation theorem [10] for the continuous mapping in Algorithm 1.  $\square$

Lemma 3 proves that there exists a feedforward network that can predict the data and pilot powers for all users in the coverage area, no matter if the users are active or not as long as Assumption 1 is satisfied. This lemma specifically proves the existence of a basic wide neural network with one hidden layer and a sufficient larger number of neurons. An equivalent narrow neural network with multiple hidden layers can be constructed by using the theoretical analysis of Lebesgue-integrable functions as in [36]. Consequently, in order to achieve highly accurate prediction performance, we base our contribution on the deep architectures of a multiple hidden layer structure [37].

### B. Convolutional Neural Network Architecture

Among all neural network structures in the literature, CNN is currently the most popular family since it achieves higher performance than fully-connected deep neural network for many applications [38], [39]. One main reason reported in [38] is that CNN effectively deduces the spectral variation existing in a dataset. In order to demonstrate why the use of CNN is suitable for power control in Massive MIMO, let us consider a squared area of 25 km<sup>2</sup> with  $L = 256$  square cells, each serving  $K_{\max} = 10$  users. The large-scale fading coefficients are generated as in Example 1, but all users are assumed to be in active mode. The interference in a real cellular system is imitated by wrap-around. We gather all the large-scale fading coefficients in a tensor

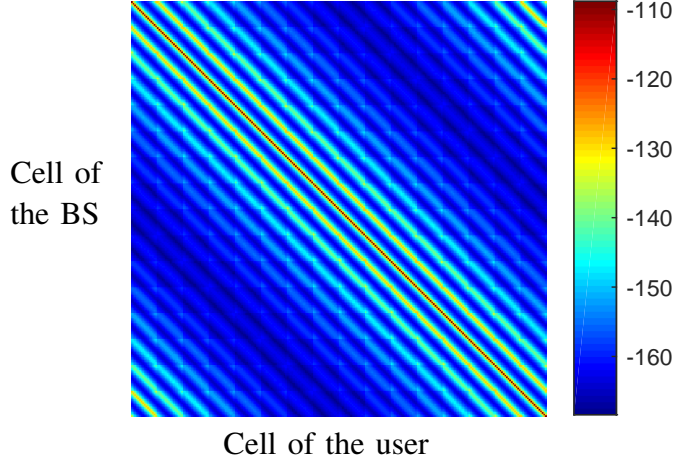


Fig. 2. The pattern created by the average large-scale fading coefficients in dB between a user in a given cell and the BS in another cell, a coverage area  $25 \text{ km}^2$  with  $L = 256$  BSs on a  $16 \times 16$  grid

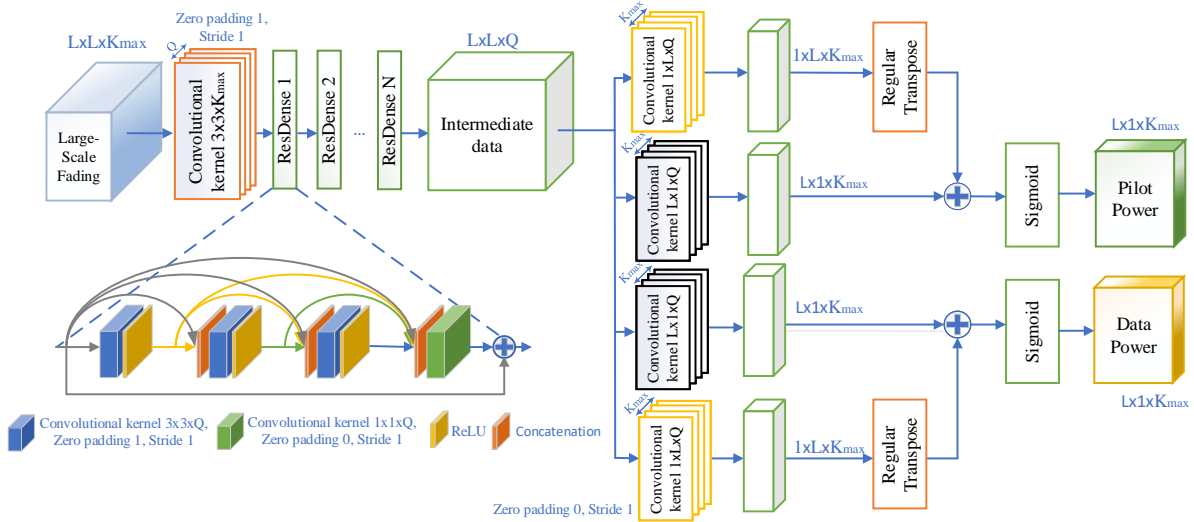


Fig. 3. The proposed PowerNet for the joint pilot and data power control from a given set of large-scale fading coefficients.

of size  $L \times L \times K_{\max}$ . For visualization, we first map this tensor to a matrix  $\mathbf{Z}$  of size  $L \times L$  by averaging over the third dimension and plot the result in Fig. 2. The number of horizontal and vertical elements is equal to  $L$ .

The color map in Fig. 2 represents the large-scale fading coefficients. For example, the color of square  $(l, j)$  represents the average large-scale fading coefficient from a user in cell  $l$  to BS  $j$ . Since there is a grid of  $16 \times 16$  cells, and the cells are numbered row by row, the large-scale fading coefficients have a certain pattern. Users in neighboring cells have larger large-scale fading coefficients than cells that are further away. The strong intensity around the main diagonal represent the cell itself and directly neighboring cells to the left or right on the same line, while the sub-diagonals with strong intensities represent neighboring cells at other lines. The other



strong intensities in the lower-left and upper-right corners are due to the wrap-around topology. A CNN can extract these patterns and utilize them to reduce the number of learned parameters significantly, compared to a conventional fully-connected network, by sharing weights and biases. Moreover, since each of the  $K_{\max}$  users in a cell have large-scale fading coefficients generated from the same distribution, a CNN can exploit this structure to reduce the number of parameters.

We will adopt the state-of-the-art residual dense block (ResDense) [40] which consists of densely connected convolutions [41] with the residual learning [42]. As shown in Fig. 3, a ResDense block inherits the Densely Connected block in [41] with residual connection to prevent the gradient vanishing problems [42]. Compared with ResDense in [40], we use additional (rectified linear unit) ReLU activation unit, i.e.,  $\xi(x) = \max(0, x)$ , after the residual connection since our mapping process only concentrates on non-negative values.

1) *The forward propagation:* From an initial set  $\mathbf{f}$ , the first component of the forward propagation is the convolutional layer

$$\mathbf{X}_1^{(m)} = \mathcal{H}_1 \left( \mathbf{l}, \left\{ \mathbf{W}_{1,j}^{(m-1)}, b_{1,j}^{(m-1)} \right\}_{j=1}^Q \right), \quad (31)$$

where  $m$  is the epoch index. The operator  $\mathcal{H}_1(\cdot, \cdot)$  denotes a series of  $Q$  convolutions [43], each using a kernel  $\mathbf{W}_{1,j}^{(m-1)} \in \mathbb{R}^{3 \times 3 \times K_{\max}}$  and a bias  $b_{1,j}^{(m-1)} \in \mathbb{R}$  to extract large-scale fading features of the input tensor  $\mathbf{l}$ .<sup>3</sup> All convolutions apply stride 1 and zero padding 1 to guarantee the same height and width between the inputs and outputs. After the first layer in (31), the feature map is a tensor with the size  $L \times L \times Q$ . Our proposed PowerNet is then constructed from  $N$  sequential connected ResDense blocks to extract special features of large-scale fading coefficients. Each ResDense block uses the four sets of convolutional kernels to extract better propagation features. The first convolution begins with  $\mathbf{X}_{2,1,4}^{(m)} = \mathbf{X}_1^{(m)}$ , then the output signal at each block of the  $n$ -th

<sup>3</sup>A convolutional layer  $\mathcal{H}(\mathbf{X}, \{\mathbf{W}_j, b_j\}_{j=1}^Q)$  defined for the tensor  $\mathbf{X} \in \mathbb{R}^{m \times n \times c}$  involves a set of  $Q$  kernels  $\mathbf{W}_j \in \mathbb{R}^{a \times b \times c}$  and  $Q$  optional biases  $b_j \in \mathbb{R}$ ,  $j = 1, \dots, Q$ , each producing an output matrix (often called feature map)  $\mathbf{G}_j \in \mathbb{R}^{m' \times n'}$  from the input  $\mathbf{X}$ . Each element  $g_j^{p,q} \in \mathbf{G}_j$  is computed as  $g_j^{p,q} = \sum_{a_1=0}^{a-1} \sum_{b_1=0}^{b-1} \sum_{c_1=0}^{c-1} \mathbf{W}_j^{a-a_1, b-b_1, c_1} \mathbf{X}^{1+s(p-1)-a_1, 1+s(q-1)-b_1, c_1} + b_j$ , where the integer parameter  $s \geq 1$  is called *stride*. Here  $m' = 1 + \lfloor \frac{m-a+2z}{s} \rfloor$ ,  $n' = 1 + \lfloor \frac{n-b+2z}{s} \rfloor$  in which  $z$  is the number of zero padding. Notice that  $\mathbf{X}$  are padded with zeros for all  $p \notin [1, m]$ ,  $q \notin [1, n]$ . The final feature map of the convolutional layer is obtained by stacking all  $\mathbf{G}_j$  together, i.e.,  $\mathbf{G} = \{\mathbf{G}_j\}_{j=1}^Q \in \mathbb{R}^{m' \times n' \times Q}$ .

ResDense block is simultaneously computed as

$$\mathbf{X}_{2,n,1}^{(m)} = \xi \left( \mathcal{H}_{2,1} \left( \mathbf{X}_{2,n-1,4}^{(m)}, \left\{ \mathbf{W}_{2,1,j}^{(m-1)} \right\}_{j=1}^Q \right) \right), \quad (32)$$

$$\mathbf{X}_{2,n,2}^{(m)} = \xi \left( \mathcal{H}_{2,2} \left( \left[ \mathbf{X}_{2,n-1,4}^{(m)}, \mathbf{X}_{2,n,1}^{(m)} \right], \left\{ \mathbf{W}_{2,2,j}^{(m-1)} \right\}_{j=1}^Q \right) \right), \quad (33)$$

$$\mathbf{X}_{2,n,3}^{(m)} = \xi \left( \mathcal{H}_{2,3} \left( \left[ \mathbf{X}_{2,n-1,4}^{(m)}, \mathbf{X}_{2,n,1}^{(m)}, \mathbf{X}_{2,n,2}^{(m)} \right], \left\{ \mathbf{W}_{2,3,j}^{(m-1)} \right\}_{j=1}^Q \right) \right), \quad (34)$$

$$\mathbf{X}_{2,n,4}^{(m)} = \mathcal{H}_{2,4} \left( \left[ \mathbf{X}_{2,n-1,4}^{(m)}, \mathbf{X}_{2,n,1}^{(m)}, \mathbf{X}_{2,n,2}^{(m)}, \mathbf{X}_{2,n,3}^{(m)} \right], \left\{ \mathbf{W}_{2,4,j}^{(m-1)} \right\}_{j=1}^Q \right), \quad (35)$$

where each operator  $\mathcal{H}_{2,i}(\cdot, \cdot)$ ,  $i \in \{1, \dots, 4\}$ , denotes a series of the  $Q$  convolutions. In the three first modules, the kernels are  $\mathbf{W}_{2,1,j}^{(m-1)} \in \mathbb{R}^{3 \times 3 \times Q}$ ,  $\mathbf{W}_{2,2,j}^{(m-1)} \in \mathbb{R}^{2 \times 3 \times 3 \times Q}$ ,  $\mathbf{W}_{2,3,j}^{(m-1)} \in \mathbb{R}^{3 \times 3 \times 3 \times Q}$ , while the remaining has  $\mathbf{W}_{2,4,j}^{(m-1)} \in \mathbb{R}^{4 \times 1 \times 1 \times Q}$ . In the first three modules, the ReLU activation function  $\xi(x)$  is used for each element. The residual dense connections in (33)–(35), which are demonstrated by concatenations, prevent the vanishing gradient problem that may often happen when some large-scale fading coefficients are small. It also helps prevent the overfitting problem by utilizing many ResDense blocks to deploy a very deep neural network.

We stress that since the input and output size of the neural network are different, multiple 1D convolutions are used to make the sides equal. In addition, to exploit correlation in both horizontal and vertical direction in the intermediate data, both horizontal and vertical 1D convolutions are used. A regular transpose layer is applied following vertical 1D convolution to ensure the data size of  $L \times 1 \times K_{\max}$ . The output of these two 1D convolutions are summed up to obtain the final prediction output. This prediction is used for both pilot and data power as depicted in Fig. 3 and is mathematically expressed as

$$\mathbf{X}_p^{(m)} = \mathcal{H}_p^v \left( \mathbf{X}_{2,N,4}^{(m)}, \left\{ \mathbf{W}_{p,j}^{v,(m-1)}, b_{p,j}^{v,(m-1)} \right\}_{j=1}^{K_{\max}} \right) + \mathcal{H}_p^h \left( \mathbf{X}_{2,N,4}^{(m)}, \left\{ \mathbf{W}_{p,j}^{h,(m-1)}, b_{p,j}^{h,(m-1)} \right\}_{j=1}^{K_{\max}} \right), \quad (36)$$

$$\mathbf{X}_d^{(m)} = \mathcal{H}_d^v \left( \mathbf{X}_{2,N,4}^{(m)}, \left\{ \mathbf{W}_{d,j}^{v,(m-1)}, b_{d,j}^{v,(m-1)} \right\}_{j=1}^{K_{\max}} \right) + \mathcal{H}_d^h \left( \mathbf{X}_{2,N,4}^{(m)}, \left\{ \mathbf{W}_{d,j}^{h,(m-1)}, b_{d,j}^{h,(m-1)} \right\}_{j=1}^{K_{\max}} \right), \quad (37)$$

where  $\mathcal{H}_p^v(\cdot, \cdot)$  and  $\mathcal{H}_p^h(\cdot, \cdot)$  denote the vertical and horizontal series of  $K_{\max}$  convolution operators dedicated to predict pilot powers by using convolutional kernels  $\mathbf{W}_{p,j}^{v,(m-1)} \in \mathbb{R}^{1 \times L \times Q}$ ,  $\mathbf{W}_{p,j}^{h,(m-1)} \in \mathbb{R}^{L \times 1 \times Q}$ ,  $\forall j$  and their related biases  $b_{p,j}^{v,(m-1)}, b_{p,j}^{h,(m-1)} \in \mathbb{R}, \forall j$ . Similar definitions for the convolution layer in (37) are made for the data powers. The feature maps from (36) and (37) are restricted in the closed unit interval  $[0, 1]$  by

$$\mathbf{X}_{p,s}^{(m)} = \text{Sigmoid} \left( \mathbf{X}_p^{(m)} \right) \quad \text{and} \quad \mathbf{X}_{d,s}^{(m)} = \text{Sigmoid} \left( \mathbf{X}_d^{(m)} \right), \quad (38)$$

where the element-wise sigmoid activation function is

$$\text{Sigmoid}(x) = \frac{1}{1 + \exp(-x)}. \quad (39)$$

Finally, the predicted pilot and data powers at epoch  $m$  are obtained by scaling up  $\mathbf{X}_{p,s}^{(m)}$  and  $\mathbf{X}_{d,s}^{(m)}$  as

$$\mathbf{O}_p^{(m)} = \mathbf{P} \odot \mathbf{X}_{p,s}^{(m)} \text{ and } \mathbf{O}_d^{(m)} = \mathbf{P} \odot \mathbf{X}_{d,s}^{(m)}, \quad (40)$$

where  $\mathbf{P} \in \mathbb{R}^{L \times 1 \times K_{\max}}$  is a collection of the maximum power budget  $P_{l,k}$  from all users with  $[\mathbf{P}]_{l,1,k} = P_{l,k}, \forall l, k$ . The operator  $\odot$  denotes the dot product of two tensors. We emphasize that the forward propagation is applied for both the training and testing phases.

2) *The back propagation:* The back propagation is only applied in the training phase. We first adopt the Frobenius norm to define the loss function as

$$f(\mathbf{f}^{(m)}) = \frac{w_1}{D} \sum_{i=1}^D \|\mathbf{O}_d^{(m),i} - \mathbf{O}_d^{\text{opt},i}\|_F^2 + \frac{w_2}{D} \sum_{i=1}^D \|\mathbf{O}_p^{(m),i} - \mathbf{O}_p^{\text{opt},i}\|_F^2 \quad (41)$$

with respect to the parameters in  $\mathbf{f}$ , where  $w_1, w_2$  are non-negative weights that balance between the total transmit power of pilot and data symbols. The loss in (41) is averaged over the training dataset  $\{\mathbf{O}_p^{\text{opt},i}, \mathbf{O}_d^{\text{opt},i}\}, i = 1, \dots, D$ , where  $D$  is the total number of large-scale fading realizations, i.e.,

The back propagation utilizes (41) to update all weights and biases in (31)–(37). PowerNet will use stochastic gradient descent [8] to obtain a good local solution to  $\Theta$ . Beginning with a random initial value  $\Theta = \Theta^{(0)}, \Delta\Theta^{(0)} = \mathbf{0}$ , and remember the current  $\Delta\Theta^{(m)}$  at each epoch  $m$ , then the update  $\Theta^{(m)}$  is

$$\Delta\Theta^{(m)} = \alpha\Delta\Theta^{(m-1)} + \eta\nabla f(\mathbf{f}^{(m-1)}), \quad (42)$$

$$\Theta^{(m)} = \Theta^{(m-1)} - \Delta\Theta^{(m)}, \quad (43)$$

where  $\alpha$  is the so-called momentum and  $\eta$  is the learning rate. We stress that the computational complexity of the back propagation can be significantly reduced if a random mini-batch  $D_t$  with  $D_t < D$  is properly selected [8] rather than processing all the training data at once.

### C. Dataset, Training, and Testing Phases

In order to train PowerNet, we use Algorithm 1 to generate training pairs of user realizations and the corresponding outputs  $\mathbf{O}_p^{\text{opt}}, \mathbf{O}_d^{\text{opt}}$  that are jointly optimized by our method presented in Algorithm 1. Specifically, we generate data with the mini-batch size  $L \times L \times K_{\max} \times D_t$  for the training and testing phase, respectively. We use the momentum and babysitting the

learning rate to get the best prediction performance and minimize the training time as well. The Adam optimization is used to train our data set [44]. PowerNet is dominated by exponentiations, divisions, and multiplications, the number of arithmetic operations required for the forward propagation at each epoch is computed as

$$9K_{\max}L^2Q + 28Q^2L^2N + 4L^2QK_{\max} + 4LK_{\max}, \quad (44)$$

which is also the exact computational complexity of the testing phase where each large-scale fading tensor only passes through the neural network once and there is no back propagation.

## V. NUMERICAL RESULTS

To demonstrate the performance of PowerNet, we consider the setup in Example 1 with  $L \in \{4, 9\}$  equally large square cells in a square area  $1 \text{ km}^2$  with wrap around. In every cell, the BS is located at the center. The distribution of users and the large-scale fading coefficients are generated according to Example 1, but the activity probability will be defined later. The maximum power level is  $P_{l,k} = 200 \text{ mW}$ ,  $\forall l, k$ . The mini-batch size is 512. The number of epochs used for the training phase is 300. We use a momentum of 0.99 and babysitting of the learning rate which varies from  $10^{-3}$  to  $10^{-5}$ . From our experiments, we note that the learning rate may be reduced by approximately three times if the test loss remains the same for 100 consecutive epochs. In the first convolutional layer, 64 kernels are used and PowerNet has 5 ResDense blocks. For the loss function in (41), we set  $w_1 = w_2 = 1$  to treat the importance of the data and pilot powers equally.

The following methods are compared:

- 1) *Fixed power (FP) level*: Each user uses the fixed maximum power level 200 mW for both pilot and data. It is denoted as FP in the figures.
- 2) *Data power optimization only (DPOO)*: The system uses a simplification of Algorithm 1 to perform data power control, while the pilot power is fixed to 200 mW. It is denoted as DPOO in the figures.
- 3) *Joint pilot and data power optimization (JPDPO)*: The system uses Algorithm 1 to jointly optimize the optimal pilot and data powers for all users. It is denoted as JPDPO in the figures.
- 4) *Joint pilot and data power optimization based on CNN (PowerNet)*: The system uses the proposed CNN described in Section IV to find the pilot and data powers for all users. It is denoted as PowerNet in the figures.
- 5) *Joint pilot and data power optimization based on fully-connected deep neural network*: The system uses a modified version of the fully-connected deep neural network in [11] to find the

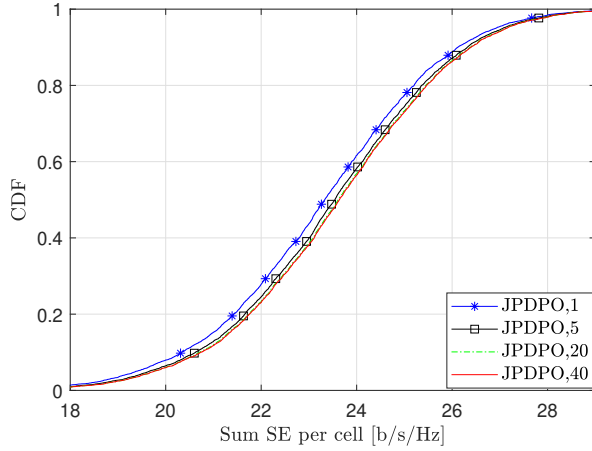


Fig. 4. CDF of sum SE per cell [b/s/Hz] versus the number of random initializations that we select the best out of. We have  $L = 4$ ,  $K_{\max} = 10$ , and  $M = 200$ . All users are in active mode with a probability  $2/3$ .

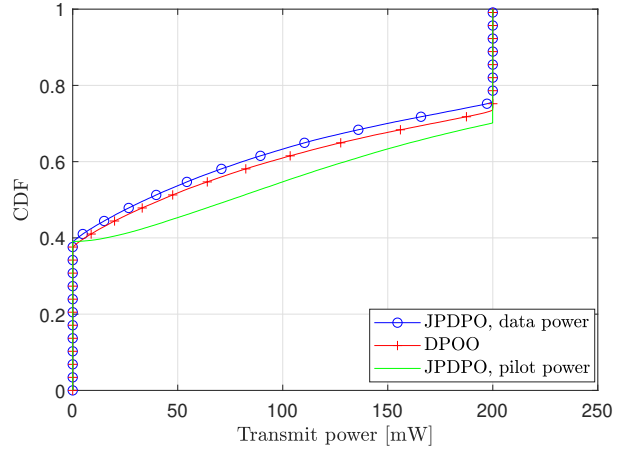


Fig. 5. CDF of pilot and data power allocation [mW] by using JPDPO and DPOO for a multi-cell Massive MIMO system with  $L = 4$ ,  $K_{\max} = 10$ , and  $M = 200$ . All users are in active mode with a probability  $2/3$ .

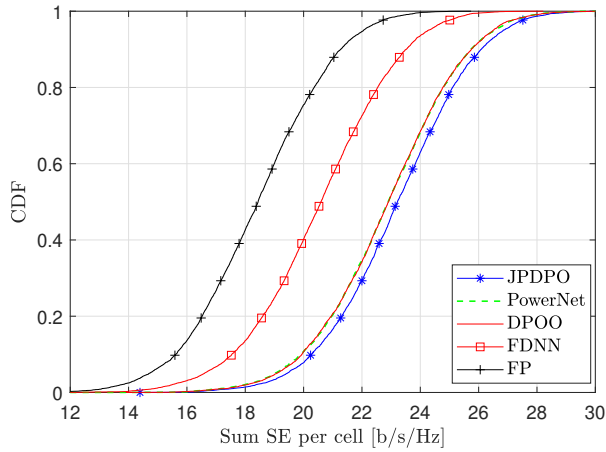


Fig. 6. CDF of sum SE per cell [b/s/Hz] with  $L = 4$ ,  $K_{\max} = 10$ , and  $M = 200$ . All users are in active mode with a probability  $2/3$ .

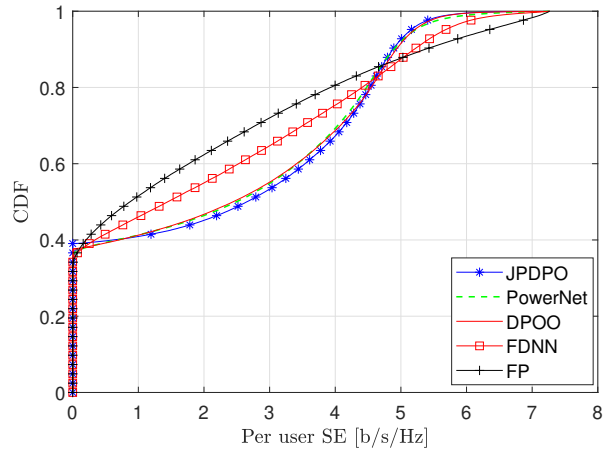


Fig. 7. CDF of per user SE [b/s/Hz] with  $L = 4$ ,  $K_{\max} = 10$ , and  $M = 200$ . All users are in active mode with a probability  $2/3$ .

optimal solution to both the pilot and data powers for all users. It is denoted as FDNN in the figures.

### A. Sum Spectral Efficiency & Power Consumption

Algorithm 1 provides a local optimum to the sum SE optimization problem, but which local optimum that is found depends on the initialization. One way to benchmark the quality of the obtained local optimum is to run the algorithm for many random initializations and take the best result. Fig. 4 shows the cumulative distribution function (CDF) of the sum SE per cell obtained from Algorithm 1 when using the best out of 1, 5, 20, or 40 different initializations.

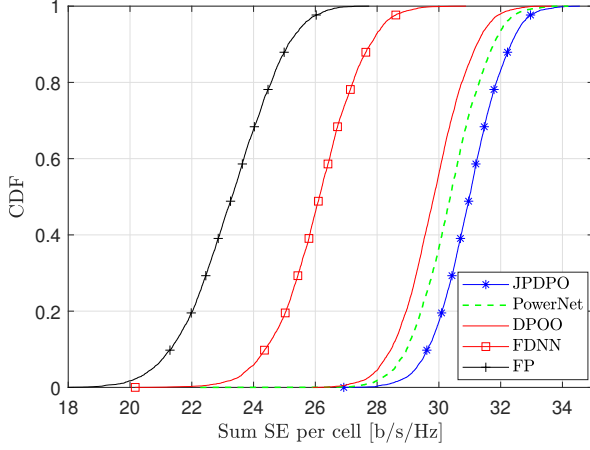


Fig. 8. CDF of sum SE per cell [b/s/Hz] with  $L = 9$ ,  $K_{\max} = 10$ , and  $M = 200$ . All users are in active mode with a probability 1.

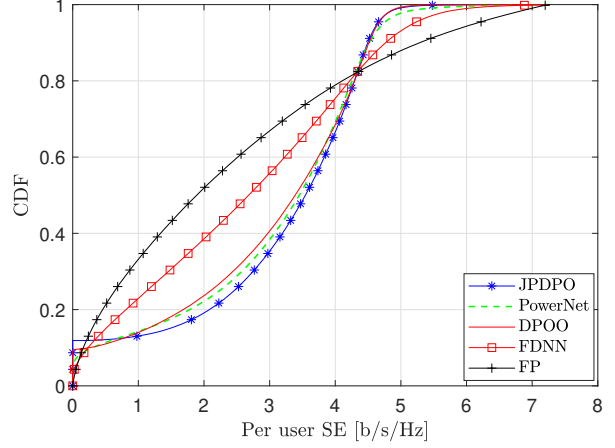


Fig. 9. CDF of per user SE [b/s/Hz] with  $L = 9$ ,  $K_{\max} = 10$ , and  $M = 200$ . All users are in active mode with a probability 1.

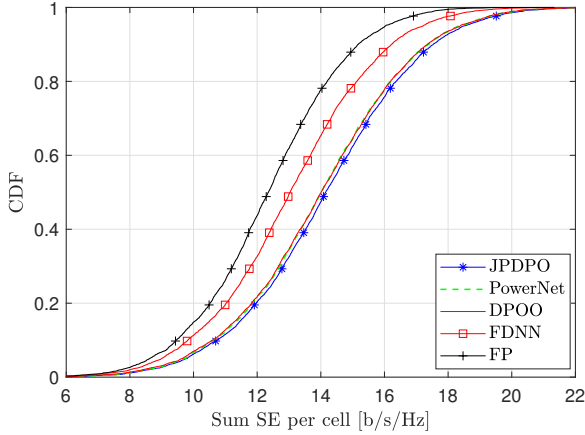


Fig. 10. CDF of SE per cell [b/s/Hz] with  $L = 4$ ,  $K_{\max} = 10$ , and  $M = 200$ . All users are in active mode with a probability  $2/3$  in the training phase and is  $1/3$  in the testing phase.

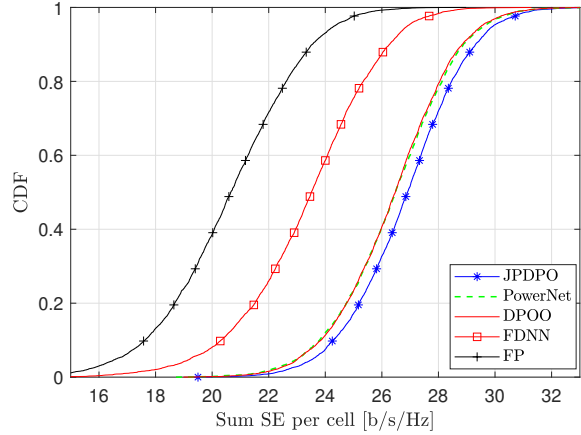


Fig. 11. CDF of SE per cell [b/s/Hz] with  $L = 4$ ,  $K_{\max} = 10$ , and  $M = 200$ . All users are in active mode with a probability  $2/3$  in the training phase and is  $5/6$  in the testing phase.

Each initial power coefficient is uniformly distributed in the range  $[0, P_{i,k}]$ . In comparison to one initialization, there are only tiny gains by spending more efforts on selecting the best out of multiple initializations. The largest relative improvement is when going from 1 to 5 initializations, but the average improvement is still less than 1%. Further increasing the number of initializations has very small impact on the sum SE. Hence, in the rest of this section, only one initialization is considered.

We show the pilot and data power coefficients produced by our proposed methods JPDPO and DPOO in Fig. 5 for the system with  $L = 4$ ,  $K_{\max} = 10$ , and  $M = 200$ . All users has the activity probability  $2/3$ . Apart from the fact that 33% of the users are inactive on the average, an additional 5% of the users are rejected from service by JPDPO due to bad channel conditions,

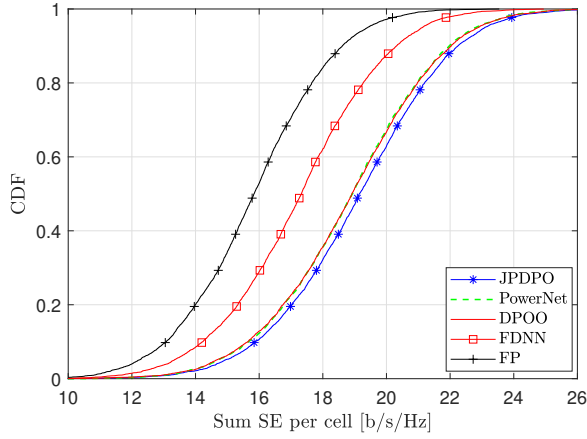


Fig. 12. CDF of SE per cell [b/s/Hz] with  $L = 4$ ,  $K_{\max} = 10$ , and  $M = 200$ . Each user has the activity probability uniformly distributed in  $[0, 1]$ .

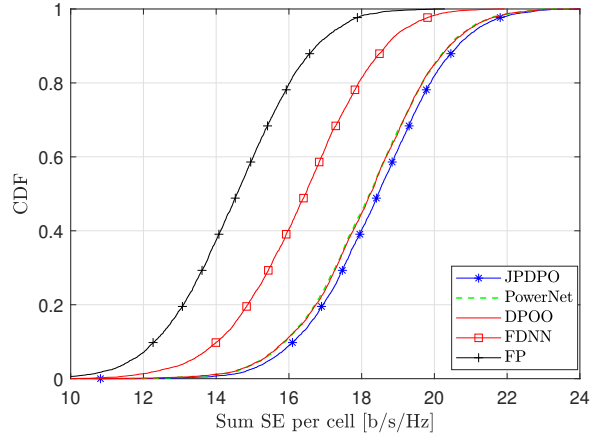


Fig. 13. CDF of SE per cell [b/s/Hz] with  $L = 4$ ,  $K_{\max} = 10$ ,  $M = 200$  for the training phase, and  $M = 100$  for the testing phase. All users are in active mode with a probability  $p = 2/3$ .

which leads to zero power when optimizing the sum SE. By utilizing JPDPO, we observe that an user in the active mode allocates 127 mW to each data symbol on average, while that is 150 mW for each pilot symbol. This 18% extra power is to improve the channel estimation quality. Even though many data and pilot symbols spend full power 200 mW to achieve the best SE, JPDPO provides 25% and 36% less power than FP. For DPOO, we are only optimizing the data power and each data symbol is allocated 124 mW.

### B. Predicted Performance of PowerNet

The CDF of sum SE per cell [b/s/Hz] is shown in Fig. 6 for a system with  $L = 4$ ,  $K_{\max} = 10$ , and  $M = 200$ . Each user has the activity probability  $2/3$ . The sum SE per cell predicted by PowerNet is almost the same as the ones obtained DPOO and it is 1.5% less than by Algorithm 1. FDNN performs 11.6% better than FP, but there is 12.9% more to reach the performance of Algorithm 1. Fig. 7 presents the prediction performance of per user SE for a four-cell system with  $K_{\max} = 10$  users. The SE obtained by PowerNet is very close to JPDPO with only about 1% loss. Fig. 7 also demonstrates that around 40% of the users are out of service, in which case no power is allocated to the training and data transmission phases.

Fig. 8 shows the CDF of sum SE per user [b/s/Hz] for the system with  $L = 9$ ,  $K_{\max} = 10$ , and  $M = 200$ , while the related case of per user SE is shown in Fig. 9. All users have the activity probability 1. FP provides the sum SE baseline of 23.26 b/s/Hz which corresponds to a per user SE of 2.33 b/s/Hz. FDNN can obtain 12.24% better average SE than the baseline. In this scenario, a 4% higher SE is achieved by optimizing both data and pilot powers, as compared

to only optimizing the data powers. Even though the number of optimization variables is much larger than in previous figures, the average prediction error of PowerNet is still very low. The improvement of PowerNet over FP is up to 16.3% for the sum SE, while it is 12.87% for the per user SE. PowerNet yields 1.78% better sum SE than JPDPO and the loss is only 2% compared with JPDPO. These results prove the scalability of PowerNet. We emphasize that there are two main reasons why PowerNet outperforms FDNN: First, PowerNet can learn better special features from multiple observations of the large-scale fading tensors by extracting the spatial correlations among BSs based on different kernels. Second, the residual dense blocks can prevent the gradient vanishing problem effectively thanks to the extra connections between the input and output of each layer.

### C. Varying User Activity

In practice, the user activity probability will change over the day, thus it is important for PowerNet to handle this without requiring retraining. Fig. 10 displays the CDF of the sum SE per cell [b/s/Hz] with 4 cells, each serving 10 users. In the training phase, each user has the activity probability  $2/3$ , while it is  $1/3$  for the testing phase. Interestingly, PowerNet still predicts the pilot and data power coefficients very well. The sum SE per cell obtained by PowerNet is almost 99% of JPDPO. Additionally, data power control is sufficient in this scenario since DPOO achieves 99% of the sum SE that is produced by JPDPO. Fig. 11 considers a more highly-loaded system with the activity probability of each user in the testing phase being  $5/6$ . There is a 30% gap between FP and JPDPO in this case. Furthermore, JPDPO brings 15% the sum SE better than FDNN. PowerNet achieves about 98.4% of what is produced by Algorithm 1.

The sum SE per cell [b/s/Hz] for a system with  $L = 4$ ,  $K_{\max} = 10$ , and  $M = 200$  is displayed in Fig. 12. In the figure, each user has its own activity probability, which is uniformly distributed in the range  $[0, 1]$ . FP yields the baseline average SE of 15.84 b/s/Hz. Meanwhile, JPDPO produces the highest SE of 19.12 b/s/Hz per cell, which is a gain of 20.71%. By only optimizing the data powers, DPOO loses 1.32% in SE over JPDPO. Importantly, PowerNet predicts the power coefficients with high accuracy and the SE is very close to JPDPO with a loss of only 1.34%. Therefore, we conclude that a single PowerNet can be trained and applied when the activity probability of users varies over time. Additionally, Fig. 13 displays the performance of a system where the number of antennas equipped at each BS in the testing phase is different from the training phase. It shows that PowerNet still provides very high prediction accuracy with the loss being only 1.30%. This indicates that PowerNet can be also applied in the scenarios where we may turn on and off antennas to improve energy-efficiency [13].



TABLE II  
 RUNTIME OF THE TESTING PHASE (POWERNET) IN MILLISECOND.

Parameter \ Mode	$L = 4, K_{\max} = 10$	$L = 9, K_{\max} = 10$	$L = 4, K_{\max} = 20$
PowerNet (CPU)	3.01	14.90	3.04
PowerNet (GPU)	0.0179	0.0283	0.0182

#### D. Runtime

To evaluate the computational complexity of PowerNet, we implement the testing phase by MatConvNet [45] with a Windows 10 personal computer having the central processing unit (CPU) AMD Ryzen 1950x 16-Core with 3.40 GHz and a Titan XP Nvidia GPU. The proposed neural network is tested using the GPU or using only the CPU. The average runtime is measured in millisecond (ms) and given in Table II. For a system with 4 cells, each serving 10 users, the runtime if using the CPU is 3.01 ms, while it is 3.04 ms if each cell has 20 users. If there are 9 cells and 10 users per cell, it requires approximately  $5\times$  and  $4.9\times$  more to obtain the solution than the system with  $L = 4, K_{\max} = 10$  or with  $L = 4, K_{\max} = 20$ , respectively. By enabling GPU mode, PowerNet can be applied for a nine-cell system ( $L = 9, K_{\max} = 10$ ) with a runtime of 0.0283 ms while taking about 0.018 ms for a four-cell system, even though the number of users per cell is up to 20 users. Hence, when using a GPU, the runtime is sufficiently low for real-time applications where each coherence interval may have a time duration of around 1 ms and therefore require sub-millisecond resource allocation decisions.

## VI. CONCLUSION

This paper has constructed a framework for the joint pilot and data power control for the sum SE maximization in uplink cellular Massive MIMO systems with a varying number of active users. This is a non-convex problem but we proposed a new iterative algorithm, inspired by the weighted MMSE approach, to find a stationary point. The joint pilot and data power optimization obtains 30% higher sum SE than equal power transmission in our simulation setup. We have used the proposed algorithm to also construct a deep neural network, called PowerNet, that predicts both the data and pilot powers very well, leading to less than 1% loss in sum SE in a multi-cell system serving 90 users.

PowerNet uses only the large-scale fading coefficients to predict the transmit power, making it scalable to Massive MIMO systems with an arbitrarily large number of antennas. It has a runtime that is far below a 1 ms, meaning that it enables real-time power control in systems where new

power control coefficients need to be obtained at the millisecond level due to changes in the scheduling decisions or user mobility. Importantly, PowerNet is designed and trained such that a single neural network can handle varying number of users per cell, which has not been the case in prior works. This demonstrates the feasibility of using deep learning for real-time power control in Massive MIMO, while still attaining basically the same performance as when solving the original problems using optimization theory. Since PowerNet is a CNN it can be easily implemented on standard specialized hardware that is developed for CNNs, while an efficient implementation of classical optimization algorithm requires the design of dedicated hardware circuits.

## APPENDIX

### A. Proof of Theorem 1

The SE of user  $k$  in cell  $l$  can be achieved by the following single-input single-output system

$$\tilde{y}_{l,k} = \sqrt{MK_{\max}\rho_{l,k}\hat{\rho}_{l,k}\beta_{l,k}^l}x_{l,k} + w_{l,k}, \quad (45)$$

where  $x_{l,k}$  is the desired real data symbol with  $\mathbb{E}\{x_{l,k}^2\} = 1$ .  $w_{l,k}$  is Gaussian noise distributed as  $\mathcal{N}(0, D_{l,k})$  with noting that  $\rho_{l,k} = \sqrt{p_{l,k}}$  and  $\hat{\rho}_{l,k} = \sqrt{\hat{p}_{l,k}}, \forall l, k$ . By using a beamforming coefficient  $u_{l,k} \in \mathbb{R}$  to detect the desired signal as

$$\hat{x}_{l,k} = u_{l,k}\tilde{y}_{l,k} = \sqrt{MK_{\max}\rho_{l,k}\hat{\rho}_{l,k}\beta_{l,k}^l}u_{l,k}x_{l,k} + u_{l,k}w_{l,k}. \quad (46)$$

The MSE of this decoding process is computed as

$$e_{l,k} = \mathbb{E}\{(x_{l,k} - \hat{x}_{l,k})^2\}. \quad (47)$$

Plugging the value  $\hat{x}_{l,k}$  in (46) into (47) and doing some algebra, we obtain the expression of  $e_{l,k}$  as in (15). For a given set  $\{u_{l,k}, \hat{\rho}_{l,k}, p_{l,k}\}$ , the optimal solution to  $u_{l,k}$  is obtained by taking the first-order derivative of  $e_{l,k}$  with respect to  $u_{l,k}$  and setting it to zero as

$$\begin{aligned} & MK_{\max}u_{l,k} \sum_{i \in \mathcal{P}_k} (\rho_{i,k})^2 (\hat{\rho}_{i,k})^2 (\beta_{i,k}^l)^2 - \sqrt{MK_{\max}\rho_{l,k}\hat{\rho}_{l,k}\beta_{l,k}^l} + \\ & u_{l,k} \left( K_{\max} \sum_{i \in \mathcal{P}_k} (\hat{\rho}_{i,k})^2 \beta_{i,k}^l + \sigma_{\text{UL}}^2 \right) \left( \sum_{i=1}^L \sum_{t \in \mathcal{A}_i} (\rho_{i,t})^2 \beta_{i,t}^l + \sigma_{\text{UL}}^2 \right) = 0. \end{aligned} \quad (48)$$

Therefore the optimal solution  $u_{l,k}^{\text{opt}}$  is computed as in (49).

$$\begin{aligned} u_{l,k}^{\text{opt}} = & \\ & \frac{\sqrt{MK_{\max}\rho_{l,k}\hat{\rho}_{l,k}\beta_{l,k}^l}}{MK_{\max} \sum_{i=1}^L \rho_{i,k}^2 \hat{\rho}_{i,k}^2 (\beta_{i,k}^l)^2 + (K_{\max} \sum_{i \in \mathcal{P}_k} \hat{\rho}_{i,k}^2 \beta_{i,k}^l + \sigma_{\text{UL}}^2) \left( \sum_{i=1}^L \sum_{t \in \mathcal{A}_i} (\rho_{i,t})^2 \beta_{i,t}^l + \sigma_{\text{UL}}^2 \right)}. \end{aligned} \quad (49)$$

The optimal value to  $w_{l,k}$  is computed by taking the first-order derivative of the objective function in problem (14) with respect to  $w_{l,k}$ , and then equating it to zero:

$$w_{l,k}^{\text{opt}} = e_{l,k}^{-1}. \quad (50)$$

Using (49) and (50) into (14), we obtain the following optimization problem

$$\begin{aligned} & \underset{\{\hat{p}_{l,k}, p_{l,k} \geq 0\}}{\text{minimize}} && \sum_{l=1}^L |\mathcal{A}_l| - \sum_{l=1}^L \sum_{k \in \mathcal{A}_l} \ln(1 + \text{SINR}_{l,k}) \\ & \text{subject to} && \hat{p}_{l,k} \leq P_{\max,l,k}, \quad \forall l, k, \\ & && p_{l,k} \leq P_{\max,l,k}, \quad \forall l, k, \end{aligned} \quad (51)$$

which is easily converted to (13), so the proof is completed.

### B. Proof of Theorem 2

For sake of simplicity, we omit iteration index in the proof. The optimal solution to  $u_{l,k}$  and  $w_{l,k}$  when the other optimization variables are fixed is respectively given in (49) and (50) with noting that  $\hat{\rho}_{l,k} = \sqrt{\hat{p}_{l,k}}$  and  $\rho_{l,k} = \sqrt{p_{l,k}}$ ,  $\forall l, k$ . The Lagrangian function of problem (14) is given by

$$\mathcal{L} = \sum_{l=1}^L \sum_{k \in \mathcal{A}_l} (w_{l,k} e_{l,k} - \ln w_{l,k}) + \sum_{l=1}^L \sum_{k \in \mathcal{A}_l} \lambda_{l,k} (\rho_{l,k}^2 - P_{\max,l,k}) + \sum_{l=1}^L \sum_{k \in \mathcal{A}_l} \mu_{l,k} (\hat{\rho}_{l,k}^2 - P_{\max,l,k}), \quad (52)$$

where  $\lambda_{l,k}$  and  $\mu_{l,k}$ ,  $\forall l, k$ , are Lagrange multipliers. In order to find the optimal solution to  $\hat{\rho}_{l,k}$  for a given set  $\{u_{l,k}, w_{l,k}, \rho_{l,k}\}$ , we take the first-order derivative of the Lagrange function with respect to this variable and equalling it to zero as

$$\begin{aligned} & \hat{\rho}_{l,k} \rho_{l,k}^2 M K_{\max} \sum_{i=1}^L w_{i,k} u_{i,k}^2 (\beta_{l,k}^i)^2 + \hat{\rho}_{l,k} K_{\max} \sum_{j=1}^L w_{j,k} u_{j,k}^2 \beta_{l,k}^j \left( \sum_{i=1}^L \sum_{t \in \mathcal{A}_i} \rho_{i,t}^2 \beta_{i,t}^j + \sigma_{\text{UL}}^2 \right) \\ & - \sqrt{M K_{\max}} \rho_{l,k} u_{l,k} w_{l,k} \beta_{l,k}^l + \lambda \hat{\rho}_{l,k} = 0. \end{aligned} \quad (53)$$

Moreover, the relationship between Lagrange multiplier  $\lambda_{l,k}$  and related variable  $\hat{\rho}_{l,k}$  is represented by the complementary slackness condition [46]

$$\lambda_{l,k} (\hat{\rho}_{l,k}^2 - P_{\max,l,k}) = 0. \quad (54)$$

Solving (53) and (54) gives us the optimal solution to  $\hat{\rho}_{l,k}$  as in (20). The global optimum to  $\rho_{l,k}$  for a given set of  $\{u_{l,k}, w_{l,k}, \hat{\rho}_{l,k}\}$  is obtained by a similar procedure.

Algorithm 1 must converge to a fixed point because the Lagrangian is a convex function constrained on one optimization variable while the other are predetermined. The objective

function of problem (14) is hence monotonically non-increasing over iterations [25]. We now prove that each stationary point of (51) is also that of problem (13). In detail, for convenience, we first reformulate problem (13) using the natural logarithm as

$$\begin{aligned} & \underset{\{\hat{\rho}_{l,k}, \rho_{l,k} \geq 0\}}{\text{maximize}} && \sum_{l=1}^L \sum_{k \in \mathcal{A}_l} \ln(1 + \text{SINR}_{l,k}) \\ & \text{subject to} && \hat{\rho}_{l,k}^2 \leq P_{l,k}, \quad \forall l, k, \\ & && \rho_{l,k}^2 \leq P_{l,k}, \quad \forall l, k, \end{aligned} \quad (55)$$

then the Lagrangian function of problem (55) is

$$\tilde{\mathcal{L}} = \sum_{l=1}^L \sum_{k \in \mathcal{A}_l} \ln(1 + \text{SINR}_{l,k}) + \sum_{l=1}^L \sum_{k \in \mathcal{A}_l} \lambda_{l,k} (\rho_{l,k}^2 - P_{\max,l,k}) + \sum_{l=1}^L \sum_{k \in \mathcal{A}_l} \mu_{l,k} (\hat{\rho}_{l,k}^2 - P_{\max,l,k}). \quad (56)$$

In order to prove the problems (49) and (14) share the same set of stationary points, it is sufficient to prove that these equalities hold for  $\forall i, t$ ,  $\partial \mathcal{L} / \partial \rho_{i,t} = \partial \tilde{\mathcal{L}} / \partial \rho_{i,t}$  and  $\partial \mathcal{L} / \partial \hat{\rho}_{i,t} = \partial \tilde{\mathcal{L}} / \partial \hat{\rho}_{i,t}$ . We prove the former which is dedicated to data power control by computing  $\partial \mathcal{L} / \partial \rho_{i,t}$  as

$$\frac{\partial \mathcal{L}}{\partial \rho_{i,t}} = \sum_{l=1}^L \sum_{k \in \mathcal{A}_l} w_{l,k} \frac{\partial e_{l,k}}{\partial \rho_{i,t}} + 2\lambda_{i,t} \rho_{i,t} \quad (57)$$

Notice that (57) holds true for  $\forall w_{l,k}$  and  $u_{l,k}$ , thus at  $w_{l,k} = w_{l,k}^{\text{opt}}$  and  $u_{l,k} = u_{l,k}^{\text{opt}}$  we obtain

$$\frac{\partial \mathcal{L}}{\partial \rho_{i,t}} = \sum_{l=1}^L \sum_{k \in \mathcal{A}_l} (e^{\text{opt}})^{-1} \frac{\partial e^{\text{opt}}}{\partial \rho_{i,t}} + 2\lambda_{i,t} \rho_{i,t} = \sum_{l=1}^L \sum_{k \in \mathcal{A}_l} \frac{\partial \text{SINR}_{l,k}}{\partial \rho_{i,t}} (1 + \text{SINR}_{l,k})^{-1} + 2\lambda_{i,t} \rho_{i,t} = \frac{\partial \tilde{\mathcal{L}}}{\partial \rho_{i,t}}. \quad (58)$$

where  $w_{l,k}^{\text{opt}} = 1/e_{l,k}^{\text{opt}}$  as a consequence of (50), while  $e_{l,k}^{\text{opt}} = (1 + \text{SINR}_{l,k})^{-1}$  is gotten by plugging (49) into (15) and doing some algebra. The procedure to get the fact that  $\partial \mathcal{L} / \partial \hat{\rho}_{i,t} = \partial \tilde{\mathcal{L}} / \partial \hat{\rho}_{i,t}$  is done in the same manner.

## REFERENCES

- [1] T. V. Chien, E. Björnson, and E. G. Larsson, "Sum spectral efficiency maximization in Massive MIMO systems: Benefits from deep learning," in *Proc. IEEE ICC*, 2019.
- [2] J. G. Andrews, S. Singh, Q. Ye, and H. S. Dhillon, "An overview of load balancing in HetNets: Old myths and open problems," *IEEE Wireless Commun. Mag.*, vol. 21, no. 2, pp. 18–25, 2014.
- [3] C. X. Wang, F. Haider, X. Gao, X. H. You, Y. Yang, D. Yuan, H. M. Aggoune, H. Haas, S. Fletcher, and E. Hepsaydir, "Cellular architecture and key technologies for 5G wireless communication networks," *IEEE Commun. Mag.*, vol. 52, no. 2, pp. 122–130, 2014.
- [4] T. L. Marzetta, "Noncooperative cellular wireless with unlimited numbers of base station antennas," *IEEE Trans. Wireless Commun.*, vol. 9, no. 11, pp. 3590–3600, 2010.

- [5] J. Jose, A. Ashikhmin, T. L. Marzetta, and S. Vishwanath, "Pilot contamination and precoding in multi-cell TDD systems," *IEEE Trans. Commun.*, vol. 10, no. 8, pp. 2640–2651, 2011.
- [6] E. Björnson, E. G. Larsson, and T. L. Marzetta, "Massive MIMO: Ten myths and one critical question," *IEEE Commun. Mag.*, vol. 54, no. 2, pp. 114 – 123, 2016.
- [7] H. V. Cheng, E. Björnson, and E. G. Larsson, "Optimal pilot and payload power control in single-cell Massive MIMO systems," *IEEE Trans. Signal Process.*, vol. 65, no. 9, pp. 2363–2378, 2017.
- [8] I. Goodfellow, Y. Bengio, and A. Courville, *Deep Learning*. MIT Press, 2016, <http://www.deeplearningbook.org>.
- [9] T. O'Shea and J. Hoydis, "An introduction to deep learning for the physical layer," *IEEE Transactions on Cognitive Communications and Networking*, vol. 3, no. 4, pp. 563–575, 2017.
- [10] K. Hornik, M. Stinchcombe, and H. White, "Multilayer feedforward networks are universal approximators," *Neural networks*, vol. 2, no. 5, pp. 359–366, 1989.
- [11] H. Sun, X. Chen, Q. Shi, M. Hong, X. Fu, and N. D. Sidiropoulos, "Learning to optimize: Training deep neural networks for interference management," *IEEE Trans. Signal Process.*, vol. 66, no. 20, pp. 5438–5453, 2018.
- [12] A. Zappone, M. Di Renzo, M. Debbah, T. T. Lam, and X. Qian, "Model-aided wireless artificial intelligence: Embedding expert knowledge in deep neural networks towards wireless systems optimization," *arXiv preprint arXiv:1808.01672*, 2018.
- [13] K. Senel, E. Björnson, and E. G. Larsson, "Joint transmit and circuit power minimization in Massive MIMO with downlink SINR constraints: When to turn on Massive MIMO?" *IEEE Trans. Wireless Commun.*, vol. 18, no. 3, 2019.
- [14] E. Björnson, J. Hoydis, and L. Sanguinetti, "Massive MIMO networks: Spectral, energy, and hardware efficiency," *Foundations and Trends® in Signal Processing*, vol. 11, no. 3-4, pp. 154–655, 2017. [Online]. Available: <http://dx.doi.org/10.1561/20000000093>
- [15] T. V. Chien, E. Björnson, and E. G. Larsson, "Joint power allocation and user association optimization for Massive MIMO systems," *IEEE Trans. Wireless Commun.*, vol. 15, no. 9, pp. 6384 – 6399, 2016.
- [16] K. Guo, Y. Guo, G. Fodor, and G. Ascheid, "Uplink power control with MMSE receiver in multi-cell MU-Massive-MIMO systems," in *Proc. IEEE ICC*, 2014, pp. 5184–5190.
- [17] T. L. Marzetta, E. G. Larsson, H. Yang, and H. Q. Ngo, *Fundamentals of Massive MIMO*. Cambridge University Press, 2016.
- [18] A. Adhikary, A. Ashikhmin, and T. L. Marzetta, "Uplink interference reduction in large-scale antenna systems," *IEEE Trans. Commun.*, vol. 65, no. 5, pp. 2194–2206, 2017.
- [19] L. Sanguinetti, A. Zappone, and M. Debbah, "Deep learning power allocation in Massive MIMO," in *Proc. ASILOMAR*, 2018.
- [20] T. V. Chien, E. Björnson, and E. G. Larsson, "Joint pilot sequence design and power control for max-min fairness in uplink Massive MIMO," in *Proc. IEEE ICC*, 2017, accepted for publication. [Online]. Available: <https://arxiv.org/abs/1703.01916>
- [21] A. Ghazanfari, E. Björnson, and E. G. Larsson, "Optimized power control for Massive MIMO with underlaid D2D communications," *IEEE Trans. Commun.*, 2019, accepted for publication.
- [22] H. T. Dao and S. Kim, "Disjoint pilot power and data power allocation in multi-cell multi-user Massive MIMO systems," *IEEE Access*, 2018.
- [23] T. X. Tran and K. C. Teh, "Network sum-rate optimization for multicell massive mimo downlink based on coordinated tilt adaptation and game theory approach," *IEEE Wireless Commun. Lett.*, vol. 5, no. 1, pp. 64–67, 2016.
- [24] X. Li, E. Björnson, E. G. Larsson, S. Zhou, and J. Wang, "Massive MIMO with multi-cell MMSE processing: Exploiting all pilots for interference suppression," *EURASIP Journal on Wireless Communications and Networking*, vol. 2017, no. 1, p. 117, 2017.
- [25] T. Van Chien, C. Mollén, and E. Björnson, "Large-scale-fading decoding in cellular Massive MIMO systems with spatially correlated channels," *IEEE Trans. Commun.*, 2018, accepted for publication. ArXiv preprint arXiv:1807.08071.
- [26] S. Kay, *Fundamentals of Statistical Signal Processing: Estimation Theory*. Prentice Hall, 1993.

- [27] L. Georgiadis, M. Neely, and L. Tassiulas, "Resource allocation and cross-layer control in wireless networks," *Foundations and Trends in Networking*, vol. 1, no. 1, pp. 1–144, 2006.
- [28] H. Al-Shatri and T. Weber, "Achieving the maximum sum rate using D.C. programming in cellular networks," *IEEE Trans. Signal Process.*, vol. 30, no. 3, pp. 1331–1341, 2012.
- [29] R. Horn and C. Johnson, *Matrix Analysis*. Cambridge University Press, 2003.
- [30] S. Christensen, R. Agarwal, E. Carvalho, and J. Cioffi, "Weighted sum-rate maximization using weighted MMSE for MIMO-BC beamforming design," *IEEE Trans. Wireless Commun.*, vol. 7, no. 12, pp. 4792–4799, 2008.
- [31] Q. Shi, M. Razaviyayn, Z.-Q. Luo, and C. He, "An iteratively weighted MMSE approach to distributed sum-utility maximization for a MIMO interfering broadcast channel," *IEEE Trans. Signal Process.*, vol. 59, no. 9, pp. 4331–4340, 2011.
- [32] P. Weeraddana, M. Codreanu, M. Latva-aho, A. Ephremides, and C. Fischione, "Weighted sum-rate maximization in wireless networks: A review," *Foundations and Trends in Networking*, vol. 6, no. 1-2, pp. 1–163, 2012.
- [33] W. Lee, M. Kim, and D.-H. Cho, "Deep power control: Transmit power control scheme based on convolutional neural network," *IEEE Commun. Lett.*, vol. 22, no. 6, pp. 1276–1279, 2018.
- [34] X. Gao, F. Tufvesson, and O. Edfors, "Massive MIMO channels—measurements and models," in *Proc. ASILOMAR*, 2013, pp. 280–284.
- [35] *Further advancements for E-UTRA physical layer aspects (Release 9)*. 3GPP TS 36.814, Mar. 2010.
- [36] Z. Lu, H. Pu, F. Wang, Z. Hu, and L. Wang, "The expressive power of neural networks: A view from the width," in *Advances in Neural Information Processing Systems*, 2017, pp. 6231–6239.
- [37] G. E. Hinton and R. R. Salakhutdinov, "Reducing the dimensionality of data with neural networks," *science*, vol. 313, no. 5786, pp. 504–507, 2006.
- [38] T. N. Sainath, B. Kingsbury, A.-r. Mohamed, G. E. Dahl, G. Saon, H. Soltau, T. Beran, A. Y. Aravkin, and B. Ramabhadran, "Improvements to deep convolutional neural networks for LVCSR," in *Proc. IEEE ASRU*, 2013.
- [39] K. Zhang, W. Zuo, Y. Chen, D. Meng, and L. Zhang, "Beyond a Gaussian denoiser: Residual learning of deep CNN for image denoising," *IEEE Trans. Image Process.*, vol. 26, no. 7, pp. 3142–3155, 2017.
- [40] Y. Zhang, Y. Tian, Y. Kong, B. Zhong, and Y. Fu, "Residual dense network for image super-resolution," in *Proc. IEEE CVPR*, 2018.
- [41] G. Huang, Z. Liu, L. Van Der Maaten, and K. Q. Weinberger, "Densely connected convolutional networks." in *Proc. IEEE CVPR*, 2017.
- [42] K. He, X. Zhang, S. Ren, and J. Sun, "Deep residual learning for image recognition," in *Proc. IEEE CVPR*, 2016.
- [43] Y. Chen, H. Jiang, C. Li, X. Jia, and P. Ghamisi, "Deep feature extraction and classification of hyperspectral images based on convolutional neural networks," *IEEE Trans. Geosci. Remote Sens.*, vol. 54, no. 10, pp. 6232–6251, 2016.
- [44] D. P. Kingma and J. Ba, "Adam: A method for stochastic optimization," in *Proc. ICLR*, 2014. [Online]. Available: <https://arxiv.org/abs/1412.6980>
- [45] A. Vedaldi and K. Lenc, "MatConvNet: Convolutional neural networks for MATLAB," in *Proc. ACM Multimedia Conference*, 2015.
- [46] S. Boyd and L. Vandenberghe, *Convex Optimization*. Cambridge University Press, 2004.